Stoch PDE: Anal Comp
https://doi.org/10.1007/s40072-021-00191-0

Behavior of solutions to the 1D focusing stochastic nonlinear Schrödinger equation with spatially correlated noise

Annie Millet[1,2] · **Alex D. Rodriguez**[3] · **Svetlana Roudenko**[3] · **Kai Yang**[3]

Received: 18 June 2020 / Revised: 27 November 2020 / Accepted: 10 February 2021

Abstract
We study the focusing stochastic nonlinear Schrödinger equation in one spatial dimension with multiplicative noise, driven by a Wiener process white in time and colored in space, in the L^2-critical and supercritical cases. The mass (L^2-norm) is conserved due to the multiplicative noise defined via the Stratonovich integral, the energy (Hamiltonian) is not preserved. We first investigate both theoretically and numerically how the energy is affected by various spatially correlated random perturbations and its dependence on the discretization parameters and the schemes. We then perform numerical investigation of the noise influence on the global dynamics measuring the probability of blow-up versus scattering behavior depending on parameters of correlation kernels. Finally, we study numerically the effect of the spatially correlated noise on the blow-up behavior, and conclude that such random perturbations do not influence the blow-up dynamics, except for shifting of the blow-up center location. This is similar to what we observed for a space-time white driving noise in Millet et al. (Numerical study of solutions behavior to the 1d stochastic L^2-critical and supercritical nonlinear Schrödinger equation, 2020. arXiv:2006.10695).

✉ Annie Millet
annie.millet@univ-paris1.fr

Alex D. Rodriguez
arodr1128@fiu.edu

Svetlana Roudenko
sroudenko@fiu.edu

Kai Yang
yangk@fiu.edu

1 SAMM (EA 4543), Université Paris 1 Panthéon Sorbonne, Centre Pierre Mendès France, 90 Rue de Tolbiac, 75013 Paris Cedex, France

2 LPSM, UMR 8001, Paris, France

3 Department of Mathematics and Statistics, Florida International University, Miami, FL 33199, USA

Published online: 14 March 2021

Keywords Stochastic NLS · Spatially correlated noise · Multiplicative noise · Blow-up probability · Blow-up dynamics · Mass-conservative numerical schemes

Mathematics Subject Classification 35R60 · 35Q55 · 60H15 · 60H35 · 65C30 · 65M06

Contents

1 Introduction

We consider the 1D stochastic focusing nonlinear Schrödinger (SNLS) equation subject to a multiplicative random perturbation.

The stochastic perturbation is driven by a Wiener process, which is *white in time* and *colored in space* and indexed by a parameter ranging from the deterministic case to space-time white noise. Previously, in [36] we considered space-time white noise, and in this paper we take a different angle and consider spatially correlated noise. Our aim is to investigate how a given type of space-colored noise influences the global behavior of solutions. On one hand we use various types of space correlations, and on the other hand—given a type of correlation structure - we observe the dependence on parameters which allows us to tune the driving noise from a regular to a rough one. In this work, we consider two types of driving noises. The *first* type is a real L^2-valued $\mathcal{Q}$-Brownian motion, where the trace-class covariance operator $\mathcal{Q}$ has a prescribed

set of eigenfunctions. The decay of the corresponding eigenvalues will be either of Gaussian type (Example 1) or polynomial type (Example 2). The *second* type of noise is spatially homogeneous, that is, defined through a convolution with a kernel creating long range interactions. In this setting the correlation kernel is either a renormalized Riesz kernel, which is singular at the origin (Example 3), or a more regular kernel with an exponential decay (Example 4). Theoretical results have been obtained only when the driving noise is white in time with a space correlation described in terms of a regular enough kernel (see e.g. [7–9,35]), while numerical investigations have been made when the diving noise is a finite approximation of a "rough" space-time white noise (see e.g. [10,11,36]). Our aim here is to investigate how *space correlation* affects solutions behavior, and in particular, the blow-up probability. When blow-up indeed occurs, we also study its dynamics, i.e., blow-up profile, rate, location.

More precisely, we study the 1D focusing stochastic NLS equation

$$\begin{cases} iu_t + u_{xx} + |u|^{2\sigma}u = \epsilon\, u \circ dW, \quad (x,t) \in \mathbb{R} \times [0,\infty), \\ u(x,0) = u_0, \end{cases} \tag{1.1}$$

where the initial condition $u_0 \in H^1(\mathbb{R})$ is deterministic and the stochastic perturbation is driven by a Wiener process W as mentioned above. The notation $u(x,t) \circ W(dt,dx)$ denotes the Stratonovich integral, which can be related to the Itô integral (using the Stratonovich-Itô correction term). For more details we refer the reader to [8, pp. 99–100] or [36, Sect. 2]. The reason for the Stratonovich integral is the L^2 norm conservation, which is important in applications. We mention that focusing stochastic NLS with multiplicative noise appears in various physical models, for example, see [1,39], also [9] and references therein.

In the deterministic case of (1.1), $\epsilon = 0$, the local wellposedness in H^1 is due to Ginibre and Velo [19,20], see also [4,25,43], and the book [3] for further details. During their lifespans, solutions to the deterministic version of (1.1) conserve mass $M(u)$ and energy (or Hamiltonian) $H(u)$ (also momentum, though it is not considered in this work), which are defined as

$$M(u(t)) \stackrel{\text{def}}{=} \|u(t)\|_{L^2}^2 = M(u_0), \tag{1.2}$$

$$H(u(t)) \stackrel{\text{def}}{=} \frac{1}{2}\|\nabla u(t)\|_{L^2}^2 - \frac{1}{2\sigma+2}\|u(t)\|_{L^{2\sigma+2}}^{2\sigma+2} = H(u_0). \tag{1.3}$$

The deterministic equation has scaling invariance: if $u(t,x)$ is a solution to (1.1) with $\epsilon = 0$, then so is $u_\lambda(t,x) = \lambda^{1/\sigma}\, u(\lambda^2 t, \lambda x)$. Under this scaling, the Sobolev H^s norm is invariant with

$$s = \frac{1}{2} - \frac{1}{\sigma}. \tag{1.4}$$

Thus, the 1D quintic ($\sigma = 2$) NLS equation is called L^2-critical ($s = 0$) and the NLS equation with $\sigma > 2$ is referred to as the L^2-supercritical ($s > 0$). In this paper we study nonlinearities with $\sigma \geq 2$ (or $s \geq 0$). In this case it is known that

H^1 solutions may blow up in finite time, by a standard convexity argument on a finite variance $V(t) \stackrel{\text{def}}{=} \int |x|^2 |u(t,x)|^2 \, dx$ (called the virial argument). Otherwise, solutions exhibit scattering (i.e., approach a linear evolution as $t \to \pm\infty$) or non-scattering (soliton) behavior, global in time. For that we recall the notion of standing waves $u(t,x) = e^{it} Q(x)$. Here, Q is the smooth, positive, decaying at infinity solution to the following equation

$$-Q + Q'' + Q^{2\sigma+1} = 0. \tag{1.5}$$

This solution is unique and called the ground state; it is explicit in 1D:

$$Q(x) = (1+\sigma)^{\frac{1}{2\sigma}} \ \operatorname{sech}^{\frac{1}{\sigma}}(\sigma x).$$

In the L^2-critical case ($\sigma = 2$) solutions exist globally in time if $M(u_0) < M(Q)$ by a result of Weinstein [44] (these solutions also scatter in L^2, see [12]). If $M(u_0) \geq M(Q)$, solutions may blow up in finite time. The minimal mass blow-up solutions, $M(u_0) = M(Q)$, were characterized by Merle [29]. The known stable blow-up dynamics is available for solutions with the initial mass larger than that of the ground state Q, and has a rich history; see [17,42,45,47] (and references therein).

In the L^2-supercritical case ($s > 0$) the known thresholds for globally existing vs. blow-up in finite time solutions depend on the scale-invariant quantities such as $M(u)^{1-s} H(u)^s$ and $\|u\|_{L^2}^{1-s} \|\nabla u(t)\|_{L^2}^s$ and their relative size to the similar quantities for the ground state Q. We summarize it in the following statement (here, $X \stackrel{\text{def}}{=} \{H^1(\mathbb{R}) \text{ if } 0 < s < 1;\ L^2(\mathbb{R}) \text{ if } s = 0\}$; also note that $s < \frac{1}{2}$ in 1D).

Theorem 1 ([12,13,16,21,23,24]) *Let $u_0 \in X$ and $u(t)$ be the corresponding solution to the 1D deterministic NLS equation (1.1) ($\epsilon = 0$) with the maximal existence interval (T_*, T^*). Suppose that*

$$M(u_0)^{1-s} H(u_0)^s < M(Q)^{1-s} H(Q)^s. \tag{1.6}$$

1. *If $\|u_0\|_{L^2}^{1-s} \|\nabla u_0\|_{L^2}^s < \|Q\|_{L^2}^{1-s} \|\nabla Q\|_{L^2}^s$, then $u(t)$ exists for all $t \in \mathbb{R}$ with $\|u(t)\|_{L^2}^{1-s} \|\nabla u(t)\|_{L^2}^s < \|Q\|_{L^2}^{1-s} \|\nabla Q\|_{L^2}^s$ and $u(t)$ scatters in X: there exist $u_\pm \in X$ such that $\lim_{t \to \pm\infty} \|u(t) - e^{it\Delta} u_\pm\|_X = 0$.*

2. *If $\|u_0\|_{L^2}^{1-s} \|\nabla u_0\|_{L^2}^s > \|Q\|_{L^2}^{1-s} \|\nabla Q\|_{L^2}^s$, then $\|u(t)\|_{L^2}^{1-s} \|\nabla u(t)\|_{L^2}^s > \|Q\|_{L^2}^{1-s} \|\nabla Q\|_{L^2}^s$ for $t \in (T_*, T^*)$. Moreover, if $|x| u_0 \in L^2(\mathbb{R})$ (finite variance), then the solution $u(t)$ blows up in finite time; if u_0 is of infinite variance, then either the solution blows up in finite time or there exists a sequence of times $t_n \to +\infty$ (or $t_n \to -\infty$) such that $\|\nabla u(t_n)\|_{L^2(\mathbb{R})} \to \infty$.*

For the extensions of Theorem 1 with (1.6) replaced by $M(u_0)^{1-s} H(u_0)^s = M(Q)^{1-s} H(Q)^s$ see [14], and by $M(u_0)^{1-s} H(u_0)^s > M(Q)^{1-s} H(Q)^s$ refer to [15,22].

The focusing NLS equation subject to a stochastic perturbation has been studied in [8] in the L^2-subcritical case, showing a global well-posedness for any $u_0 \in H^1$

for a driving noise with a sufficiently regular space correlation. Blow-up for $0 \leq s < 1$ has been studied in [9] for a multiplicative stochastic perturbation driven by a Wiener process, which is white in time and with regular enough space correlation. The results in [9] state that for $s \geq 0$ initial data with finite variance ($V(0) < \infty$) and sufficiently negative energy blow up before some finite time $t > 0$ with positive probability [7, Thm 4.1]. In the L^2-supercritical case, the stochastic perturbation can create blow up with strictly positive probability from *any* initial condition before any strictly positive time, see [9, Thm 5.1]. More precisely, if the noise is nondegenerate, i.e., $\ker \phi^* = \{0\}$, and regular enough, then for any non-trivial initial data $u_0 \in \Sigma^2$ (here, $\Sigma^2 = \{f \in H^2 : |x|^2 u \in L^2\}$) and any time $t > 0$, a blow-up occurs with strictly positive probability before time t. Indeed, the non-degeneracy of the noise implies that before any prescribed positive time (say $T/2$), the solution $u(t)$ will be (with strictly positive probability) in any given neighborhood of a function v such that the deterministic NLS equation starting from v will blow up before time $T/2$.

One major difference (and difficulty) compared to the deterministic setting is that energy is not necessarily conserved in the stochastic perturbations. In the SNLS equation (1.1) with multiplicative noise (defined via the Stratonovich integral) the mass is conserved a.s., see [8], which allows to prove global existence of solutions in the L^2-critical setting with $M(u_0) < M(Q)$; see [35]. To further understand global behavior in the L^2-supercritical setting one needs to control energy (as can be seen from Theorem 1). Due to the scaling invariance and mass conservation, in [35] an analog of Theorem 1 is obtained to describe behavior of solutions on some (random) time interval in the stochastic setting of the L^2-critical and supercritical cases. In particular, if $M(u_0)^{1-s} H(u_0)^s < \gamma\, M(Q)^{1-s} H(Q)^s$ for some $\gamma \in (0, 1)$, and $\|u_0\|_{L^2}^{1-s} \|\nabla u_0\|_{L^2}^s < \|\nabla Q\|_{L^2}^{1-s} \|\nabla Q\|_{L^2}^s$, then there is no blow-up until some random time $\tau^*(u_0)$ such that $P(\tau^*(u_0) > T) > 0$ for $T < T^*$, where $T^* = T^*(\sigma, \gamma, M(u_0), M(Q), m_\phi)$, and where the constant m_ϕ defined in (2.4) is related to the roughness and strength of the driving noise W.

While it is possible to obtain certain upper bounds for the energy on a (random) time interval, the exact behavior of the energy is not yet understood. This is one of the motivations for this work, namely, to investigate the time evolution of energy, at least in the discretized setting. We then investigate solutions behavior with various initial data by carefully tracking time evolution numerically, this also allows us to study the dependence on different space correlations of the driving noise. Another motivation is to see how the considered noise (colored in space and white in time) affects the probability of blow-up (vs. global existence), and then finally, how noise affects the blow-up dynamics, compared with the deterministic case. Therefore, we first introduce the discretization of energy (as well as mass), then obtain *theoretical* bounds on that discrete analog, including the dependence on various discretization and perturbation parameters. After that we continue with *numerical* studies: (i) we track the evolution of energy, (ii) we then study behavior of solutions and how the noise either prevents blow-up, or leads towards it, and (iii) we investigate the blow-up dynamics of solutions in both L^2-critical and L^2-supercritical settings, obtaining rates, profiles and location of blow-up. One advantage of the noise setting in this paper is that we can tune parameters range from an almost deterministic situation with a regular noise to that of a very rough driving Wiener process, such as space-time white noise,

that we studied in [36]. Before we further discuss our findings, we review the known deterministic results for the stable NLS blow-up dynamics (for further overview see [17,42,45,46]).

A stable blow-up in deterministic setting exhibits a self-similar structure with specific rates and profiles. Due to the scaling invariance, the following rescaling of the (deterministic) equation is introduced via the new space and time coordinates (τ, ξ) and a scaling function $L(t)$ (for more details see [27,42,46])

$$u(t,r) = \frac{1}{L(t)^{\frac{1}{\sigma}}} v(\tau,\xi), \quad \text{where} \quad \xi = \frac{r}{L(t)}, \quad r = |x|, \quad \tau = \int_0^t \frac{ds}{L(s)^2}. \tag{1.7}$$

The Eq. (1.1) (with $\epsilon = 0$) then becomes

$$i v_\tau + i a(\tau) \left(\xi v_\xi + \frac{v}{\sigma} \right) + \Delta v + |v|^{2\sigma} v = 0, \tag{1.8}$$

with

$$a(\tau) = -L \frac{dL}{dt} \equiv -\frac{d \ln L}{d\tau}. \tag{1.9}$$

The limiting behavior of the parameter $a(\tau)$ in (1.8) as $\tau \to \infty$ makes a significant difference in blow-up behavior between the L^2-critical and L^2-supercritical cases. As $a(\tau)$ is related to $L(t)$ via (1.9), the behavior of the rate, $L(t)$, is typically studied to understand the blow-up behavior (we do so in Sect. 5). Separating variables $v(\tau, \xi) = e^{i\tau} Q(\xi)$ in (1.8) and assuming that $a(\tau)$ converges to a constant a, the following system is used to obtain blow-up profiles

$$\begin{cases} Q_{\xi\xi} - Q + ia \left(\dfrac{Q}{\sigma} + \xi Q_\xi \right) + |Q|^{2\sigma} Q = 0, \quad \xi \in [0, \infty), \\ Q_\xi(0) = 0, \quad Q(0) \in \mathbb{R}, \quad Q(\infty) = 0. \end{cases} \tag{1.10}$$

Besides the conditions above, it is also required to have $|Q(\xi)|$ decrease monotonically with ξ, without any oscillations as $\xi \to \infty$ (see more on that in [2,42,46]). In the L^2-critical case the above equation is simplified (due to a being zero) to the ground state (1.5). Nevertheless, the Eq. (1.10) with nonzero a (but asymptotically approaching zero) is investigated (even in the L^2-critical context), since the correction in the blow-up rate $L(t)$ comes exactly from that. It should be emphasized that the decay of $a(\tau)$ to zero in the critical case is extremely slow, which makes it very difficult to pin down the exact blow-up rate, or more precisely, the correction term in the blow-up rate. In fact it was quite some time until rigorous analytical proofs appeared (in 1D [37], followed by a systematic work in [18–32] and references therein; see [42] or [46, Introduction]). In the L^2-supercritical case, the convergence of $a(\tau)$ to a non-zero constant is rather fast, and the rescaled solution converges to the blow-up profile fast as well. The more difficult question in this case is the profile itself, since it is no longer the ground state from (1.5), but exactly an admissible solution (without fast oscillating decay and with an asymptotic decay of $|\xi|^{-\frac{1}{\sigma}}$ as $|\xi| \to \infty$) of (1.10).

Among all admissible solutions to (1.10) there is no uniqueness as it was shown in [2,26,46]. These solutions generate branches of so-called multi-bump profiles, that are labeled $Q_{J,K}$, indicating that the Jth branch converges to the Jth excited state, and K is the enumeration of solutions in a branch. The solution $Q_{1,0}$, the first solution in the branch $Q_{1,K}$ (this is the branch, which converges to the L^2-critical ground state solution Q in (1.5) as the critical index $s \to 0$), is shown (numerically) to be the profile of a stable supercritical blow-up. The third and fourth authors have been able to obtain the profile $Q_{1,0}$ in various NLS cases (see [46], also an adaptation for a nonlocal Hartree-type NLS [47]), and thus, we are able to use that in this work and compare it with the stochastic case.

In the focusing SNLS case, in [10,11] numerical simulations were done when the driving noise is rough, namely, it is an approximation of space-time white noise. The effect of the multiplicative (and also additive) noise is described for the propagation of solitary waves. In particular, it was noted that the blow-up mechanism transfers energy from the larger scales to smaller scales, thus, allowing the mesh size to affect the formation of the blow-up in the case of multiplicative noise (the coarse mesh allows formation of blow-up and the finer mesh prevents it or delays it). There the authors investigated the probability of the blow-up time and they observed that in the multiplicative case the blow-up is delayed on average. Other parameters' dependence (such as the dependence on the strength ϵ of the noise) is also discussed.

In this paper we use *three* numerical schemes from [36], where we applied them to study the SNLS with space-time white noise. This lets us track the energy of the stochastic Schrödinger flow in each of the four examples of regular noise driving the multiplicative perturbation. After that we investigate the influence of the noise on the global behavior, in particular, probability of blow-up depending on the strength of the noise and type of spatial correlation. In particular, we confirm that the noise generally delays or prevents blow-up. The more regular the noise is, the less delay or preventing effect it will have on the blow-up solutions. Finally, we study the influence of the spatially correlated noise on the blow-up dynamics. In particular, we investigate the following conjectures of blow-up dynamics in SNLS:

Conjecture 1 (L^2-critical case) *Let $u_0 \in H^1(\mathbb{R})$ and $u(t)$, $t > 0$, be the solution to the SNLS equation (1.1) with $\sigma = 2$ and the multiplicative noise $\epsilon\, u \circ dW$ driven by a spatially-correlated Brownian motion W.*

Sufficiently localized initial data with $\|u_0\|_{L^2} > \|Q\|_{L^2}$ blows up in finite positive (random) time with positive probability.

If a solution blows up at a random positive time $T(\omega) > 0$ for a given $\omega \in \Omega$, then the blow-up is characterized by a self-similar profile (same ground state profile Q from (1.5) as in the deterministic NLS), and for t close to $T(\omega)$

$$\|u_x(t,\cdot)\|_{L^2_x} \sim \frac{1}{L(t)}, \quad \text{where} \quad L(t) \sim \left(\frac{2\pi(T-t)}{\ln|\ln(T-t)|}\right)^{\frac{1}{2}} \quad \text{as} \quad t \to T(\omega), \tag{1.11}$$

known as the log-log rate due to the double logarithmic correction in $L(t)$.

Thus, the solution blows up in a self-similar regime with profile converging to a rescaled ground state profile Q, and the core part of the solution $u_c(x,t)$ behaves as

$$u_c(t,x) \sim \frac{1}{L(t)^{\frac{1}{2}}} Q\left(\frac{x-x(t)}{L(t)}\right) e^{i\gamma(t)}$$

with $L(t)$ converging as in (1.11), $\gamma(t) \to \gamma_0$, and $x(t) \to x_c$ (the blow-up center).

Furthermore, conditionally on the existence of blow-up in finite time $T(\omega) > 0$, x_c is a Gaussian random variable.

Conjecture 2 (L^2-supercritical case) *Let $u_0 \in H^1(\mathbb{R})$ and $u(t)$, $t > 0$, be the solution to the SNLS equation (1.1) with $\sigma > 2$ and the multiplicative noise $\epsilon\, u \circ dW$ driven by a spatially-correlated Brownian motion W.*

Sufficiently localized initial data blows up in finite positive (random) time with positive probability.

If a solution blows up at a random positive time $T(\omega) > 0$ for a given $\omega \in \Omega$, then the blow-up core dynamics $u_c(x,t)$ for t close to $T(\omega)$ is characterized as

$$u_c(t,x) \sim \frac{1}{L(t)^{\frac{1}{\sigma}}} Q\left(\frac{x-x(t)}{L(t)}\right) \exp\left(i\theta(t) + \frac{i}{2a(t)} \log\frac{T}{T-t}\right), \qquad (1.12)$$

where the blow-up profile Q is the $Q_{1,0}$ solution of the Eq. (1.10), $a(t) \to a$, the specific constant corresponding to the $Q_{1,0}$ profile, $\theta(t) \to \theta_0$, $x(t) \to x_c$ (the blow-up center), and $L(t) = (2a(T-t))^{\frac{1}{2}}$. Consequently, a direct computation yields that for t close to $T(\omega)$

$$\|u_x(t,\cdot)\|_{L^2_x} \sim \frac{1}{L(t)^{1-s}} = (2a(T-t))^{-\frac{1}{2}(\frac{1}{2}+\frac{1}{\sigma})}. \qquad (1.13)$$

Furthermore, conditionally on the existence of blow-up in finite time $T(\omega) > 0$, x_c is a Gaussian random variable.

Thus, the blow-up happens with a polynomial rate (1.13) without correction, and with profile converging to the same blow-up profile as in the deterministic supercritical NLS case.

We note that in the deterministic setting the stable blow-up behavior is conjectured as above (except for the location, since it is only relevant to the stochastic case). In the L^2-critical setting, Conjecture 1 is proved in the case when the initial mass is slightly above the mass of the ground state Q and has negative energy (see [30–32,38] and references therein), provided the spectral property holds (which in low dimensions was proved with the numerically-assisted proof in [18] and the latest results are available up to $d \leq 12$ by the work of the third and fourth authors in [45] with further blow-up rate and profile studies). In the L^2-supercritical setting, for Conjecture 2, there are no analytical proofs of stable blow-up (except for a slightly supercritical case, see [33,34]), since there is no analytical description of solutions to the profile equation (1.10) (see works for a slightly supercritical profile in [26,40,41]). Numerical investigations are

done in [2] and by the last two authors in [46] for the dimensions $2 \leq d \leq 7$ (see also [47]). Having the available tools and methods from the deterministic setting, we are able to postulate Conjectures 1 and 2 and provide some numerical justification.

Previously, we confirmed the above conjectures in the case of a driving space-time white noise W (for both additive and multiplicative perturbations) in [36]. Here, we are also able to confirm the above conjectures in the setting of this paper - the four examples of spatially correlated Wiener processes, which are used to define the multiplicative random perturbations (see discussion in Sect. 6).

The paper is organized as follows. In Sect. 2 we review the mass conservation and energy bounds in the stochastic setting, then recall the three mass-conservative numerical schemes, one of them being also energy-conservative in the deterministic setting. In Sect. 3 we describe the first type of the driving noise W, which is a $\mathcal{Q}$-Brownian motion, via two examples. This is accompanied by deriving upper estimates for energy in both examples, and then numerical tracking of energy. In Sect. 4 we study a spatially homogeneous noise W via another two examples, observing in our simulations initially the growth and then leveling off of the energy as in the case of $\mathcal{Q}$-Brownian motions. After that we investigate numerically the probability of blow-up in Sect. 5 and how it is influenced by the strength of the noise and a spatial correlation parameter. Our investigations of profiles, rates and center location in the blow-up dynamics are in Sect. 6. We give conclusions in Sect. 7 with an appendix containing our computations for the normal distribution of the random variable representing the location shift of the blow-up center.

2 Preliminaries

In this section we recall the time evolution of mass and energy when Eq. (1.1) is driven by a regular noise, then define the numerical schemes and the discretized versions of the mass and energy.

2.1 Time dependence of mass and energy

Let the noise $W = \sum_{j\geq 0} \beta_j \phi e_j$ be real-valued and regular in the space variable, that is, colored in space by means of a Hilbert–Schmidt operator ϕ from $L^2_{\mathbb{R}}(\mathbb{R})$ to $L^2_{\mathbb{R}}(\mathbb{R})$, with the Hilbert–Schmidt norm denoted by $\|\phi\|_{L^{0,0}_{2,\mathbb{R}}}$. Since the process W is real-valued and the noise is multiplicative, as in the deterministic case, i.e., when $\epsilon = 0$, the Eq. (1.1) conserves mass almost surely (see [8, Proposition 4.4]), i.e.,

$$M(u(t)) = \int_{\mathbb{R}} |u(t,x)|^2 dx = M(u_0) \quad \text{a.s.} \tag{2.1}$$

This is a consequence of rewriting (1.1) using the Stratonovich-Itô correction term

$$i d_t u(t) - \big(\Delta u(t) + |u(t)|^{2\sigma} u(t)\big) dt = u(t) dW(t) - \frac{i}{2} F_\phi u(t) dt, \tag{2.2}$$

where $F_\phi(x) = \sum_{k\geq 0} \left(\phi e_k(x)\right)^2$, and applying the Itô formula.

In the deterministic case, the energy (or Hamiltonian) $H(u)$ of the solution, defined in (1.3), is conserved in time. This is no longer true in a stochastic setting.

In order to study the time evolution of energy in the stochastic framework, we have to impose stronger assumptions on the operator ϕ. More precisely, we require that ϕ is Hilbert–Schmidt from $L^2_{\mathbb{R}}(\mathbb{R})$ to $H^1_{\mathbb{R}}(\mathbb{R})$, and Radonifying from $L^2_{\mathbb{R}}(\mathbb{R})$ to $W^{1,\kappa}_{\mathbb{R}}(\mathbb{R})$ for some $\kappa > 2$. As proved in [8, Proposition 4.5], the stochastic perturbation creates a time evolution of energy described by the Itô formula for the Itô formulation (2.2) of the stochastic NLS equation (1.1)

$$H(u(t)) = H(u_0) - \operatorname{Im} \epsilon \sum_{j\geq 0} \int_0^t \int_{\mathbb{R}} \bar{u}(s,x)\nabla u(s,x)\cdot(\nabla\phi e_j)(x)dxd\beta_j(s) + \frac{\epsilon^2}{2}\sum_{j\geq 0}\int_0^t\int_{\mathbb{R}} |u(s,x)|^2\,|\nabla(\phi e_j)|^2 dxds.$$

Taking expected values, we deduce that for any $\epsilon > 0$

$$\begin{aligned}\mathbb{E}(H\big(u(t)\big) &= H(u_0) + \frac{\epsilon^2}{2}\mathbb{E}\sum_{j\geq 0}\int_0^t\int_{\mathbb{R}} |u(s,x)|^2\big|(\nabla\phi e_j)(x)\big|^2 dxds \\ &\leq H(u_0) + \frac{\epsilon^2}{2} m_\phi M(u_0)\, t, \end{aligned} \tag{2.3}$$

where

$$m_\phi \stackrel{\text{def}}{=} \sup_{x\in\mathbb{R}} \sum_{j\geq 0} |\nabla(\phi e_j)(x)|^2 < \infty, \tag{2.4}$$

since ϕ is Radonifying from $L^2_{\mathbb{R}}(\mathbb{R})$ to $\dot{W}^{1,\infty}_{\mathbb{R}}(\mathbb{R})$.

We next describe our discretizations and the numerical schemes that we use, which preserve the discrete mass; we use those to study the effect of various types of space-correlated driving noises on the global behavior of solutions, including the blow-up probability before a given time T and the blow-up profiles. The time evolution of energy is a crucial first step in this study.

2.2 Discretizations and numerical schemes

Let $[-L_c, L_c]$ to be a symmetric interval of computational domain, and let $\{x_j\}_{j=0}^N$ be grid points from $-L_c$ to L_c (the points x_j are not necessarily equi-distributed); denote $\Delta x_j = x_{j+1} - x_j$. We also use the pseudo-points x_{-1} satisfying $\Delta x_{-1} = \Delta x_0$, and x_{N+1} satisfying $\Delta x_{N-1} = \Delta x_N$. Note that $x_0 = -L_c$, $x_N = L_c$, and in the case of a constant space mesh Δx, and for N even we have $x_{\frac{N}{2}} = 0$ and $x_{\frac{N}{2}-k} = -x_{\frac{N}{2}+k}$ for $k = 0, \ldots, \frac{N}{2}$.

We recall the second order discrete differential operators for a non-constant space mesh; it replaces ∂_{xx} (see [36] for more details). Given a function $f : [-L_c, L_c] \to \mathbb{C}$, set $f_j = f(x_j)$, and from the Taylor expansion of $f(x_{j-1})$ and $f(x_{j+1})$ around x_j, one can define the second order difference operator, which is a second order approximation of ∂_{xx}, as

$$\mathcal{D}_2 f_j \stackrel{\text{def}}{=} \frac{2}{\Delta x_{j-1}(\Delta x_{j-1} + \Delta x_j)} f_{j-1} - \frac{2}{\Delta x_{j-1}\Delta x_j} f_j + \frac{2}{(\Delta x_{j-1} + \Delta x_j)\Delta x_j} f_{j+1}. \tag{2.5}$$

Let $\Delta t_m = t_{m+1} - t_m$ be the time step size from $t = t_m$ to $t = t_{m+1}$, $m = 0, 1, \ldots$, and u_j^m denote the full discretization in space and time of u at time t_m and location x_j, that is, the approximation of $u(t_m, x_j)$. Set $V_j^m \stackrel{\text{def}}{=} |u_j^m|^{2\sigma}$, and define the mid-point in time as $u_j^{m+\frac{1}{2}} = \frac{1}{2}(u_j^m + u_j^{m+1})$.

In Sects. 3 and 4, simulations are done on a uniform space mesh Δx (that is, $\Delta x_j = \Delta x$ for all j). Later in the paper, where we investigate global behavior and track the blow-up dynamics in Sects. 5 and 6, our mesh-refinement algorithm leads to a non-uniform mesh. Therefore, we give our schemes in terms of non-uniform meshes.

We use the following discretization schemes from [36]: the mass-energy conservative (MEC) scheme (which is a generalization of the scheme in [11] to the non-uniform mesh)

$$i\,\frac{u_j^{m+1} - u_j^m}{\Delta t_m} + \mathcal{D}_2 u_j^{m+\frac{1}{2}} + \frac{1}{\sigma+1}\,\frac{|u_j^{m+1}|^{2(\sigma+1)} - |u_j^m|^{2(\sigma+1)}}{|u_j^{m+1}|^2 - |u_j^m|^2}\,u_j^{m+\frac{1}{2}} = \epsilon f_j^{m+\frac{1}{2}}, \tag{2.6}$$

the Crank–Nicholson (CN) scheme

$$i\,\frac{u_j^{m+1} - u_j^m}{\Delta t_m} + \mathcal{D}_2 u_j^{m+\frac{1}{2}} + V_j^{m+\frac{1}{2}} u_j^{m+\frac{1}{2}} = \epsilon f_j^{m+\frac{1}{2}}, \tag{2.7}$$

and our linear extrapolation (LE) scheme, which uses the extrapolation to approximate the potential term $V_j^{m+\frac{1}{2}}$, namely,

$$i\,\frac{u_j^{m+1} - u_j^m}{\Delta t_m} + \mathcal{D}_2 u_j^{m+\frac{1}{2}} + \frac{1}{2}\left(\frac{2\Delta t_{m-1} + \Delta t_m}{\Delta t_{m-1}} V_j^m - \frac{\Delta t_m}{\Delta t_{m-1}} V_j^{m-1}\right) u_j^{m+\frac{1}{2}} = \epsilon f_j^{m+\frac{1}{2}}. \tag{2.8}$$

The Neumann boundary conditions on both sides of the space interval are imposed by setting $u_{-1} = u_0$ and $u_N = u_{N+1}$ on the pseudo-points x_{-1} and x_{N+1}.

We set the stochastic perturbation as

$$f_j^{m+\frac{1}{2}} \stackrel{\text{def}}{=} \frac{1}{2}(u_j^m + u_j^{m+1})\,\tilde{f}_j^{m+\frac{1}{2}}, \tag{2.9}$$

where $\tilde{f}_j^{m+\frac{1}{2}}$ depends on the type of driving noise (four different examples), which we describe next.

3 Stochastic perturbation driven by a $\mathcal{Q}$-Wiener process

3.1 Description of the driving noise

Let $\mathcal{Q}$ be a trace-class positive operator from $L^2_{\mathbb{R}}(\mathbb{R})$ to itself. Recall that a $\mathcal{Q}$-Wiener process $W = \{W(t)\}_{t\geq 0}$ is an $L^2_{\mathbb{R}}(\mathbb{R})$-valued process with continuous trajectories, independent time increments, with $W(0) = 0$, and such that the distribution of $W(t) - W(s)$ is Gaussian with mean zero and covariance operator $(t-s)\mathcal{Q}$ on $L^2_{\mathbb{R}}(\mathbb{R})$ for $0 \leq s \leq t$. This implies that given instants $s, t \in [0, +\infty)$ and functions $u, v \in L^2_{\mathbb{R}}(\mathbb{R})$,

$$\mathbb{E}\big[(W(s), u)\ (W(t), v)\big] = (s\hat{t})\ (\mathcal{Q}u, v).$$

Let $\{e_j\}_{j\geq 0}$ be an orthonormal basis of $L^2_{\mathbb{R}}(\mathbb{R})$ such that $\mathcal{Q}\,e_j = \lambda_j e_j$ for $j \geq 1$. Then $\lambda_j > 0$ and $\sum_{j\geq 0}\lambda_j < \infty$. Note that the processes

$$\beta_j(t) \stackrel{\text{def}}{=} \frac{1}{\sqrt{\lambda_j}}\big(W(t), e_j\big), \quad t \geq 0, \quad j = 1, 2, \ldots,$$

are independent one-dimensional standard Brownian motions. Let $\phi : L^2_{\mathbb{R}}(\mathbb{R}) \to L^2_{\mathbb{R}}(\mathbb{R})$ be the Hilbert–Schmidt operator defined by $\phi\, e_j = \sqrt{\lambda_j} e_j$. Then the Wiener process W can be expanded as follows

$$W(t) = \sum_{j\geq 0} \sqrt{\lambda_j}\,\beta_j(t)\,e_j = \sum_{j\geq 0} \beta_j(t)\phi\, e_j. \tag{3.1}$$

We send the reader to [5] for further details.

For practical reasons we only consider finitely many orthonormal functions $\{e_j\}_{0\leq j\leq N}$, thus, truncate the series in (3.1) accordingly. This defines an approximation W_N of W, namely, $W_N(t) = \sum_{j=0}^N \beta_j(t)\phi\, e_j$. In order to study the energy, we need the operator ϕ to be Hilbert–Schmidt from $L^2_{\mathbb{R}}(\mathbb{R})$ to $H^1_{\mathbb{R}}(\mathbb{R})$, and thus, require the functions $\{e_j\}$ to belong to $H^1_{\mathbb{R}}(\mathbb{R})$. In the same spirit as in [36], we consider "hat" functions $\{g_j\}_{j\geq 0}$ defined on the space interval $[x_j, x_{j+1}]$ as follows. Let

$x_{j+\frac{1}{2}} = \frac{1}{2}[x_j + x_{j+\frac{1}{2}}]$, $\Delta x_j = x_{j+1} - x_j$, and for $j = 0, \ldots, N-1$, set

$$g_j(x) \stackrel{\text{def}}{=} \begin{cases} c_j(x - x_j) & \text{for} \quad x \in [x_j, x_{j+\frac{1}{2}}], \\ c_j(x_{j+1} - x) & \text{for} \quad x \in [x_{j+\frac{1}{2}}, x_{j+1}], \end{cases}$$

where $c_j \stackrel{\text{def}}{=} \frac{2\sqrt{3}}{(\Delta x_j)^{3/2}}$ is chosen to ensure $\|g_j\|_{L^2} = 1$.

Given points $x_0 < x_1 < \cdots < x_N$, define the functions e_j's, $j = 0, \ldots, N$, by

$$\begin{cases} e_j = \ g_{j-1} 1_{[x_{j-\frac{1}{2}}, x_j]} + g_j 1_{[x_j, x_{j+\frac{1}{2}}]}, \ 1 \le j \le N-1, \\ e_0 = \ \sqrt{2}\, g_0 1_{[x_0, x_{\frac{1}{2}}]}, \quad e_N = \sqrt{2}\, g_{N-1} 1_{[x_{N-\frac{1}{2}}, x_N]}. \end{cases} \tag{3.2}$$

Since the functions $\{e_j\}_{j=0}^N$ have disjoint supports, they are orthogonal. By symmetry of the functions g_j, we have $\|e_j\|_{L^2} = 1$ for $j = 0, \ldots, N$. We can now construct an orthonormal basis $\{e_k\}_{k \ge 0}$ of $L^2_{\mathbb{R}}(\mathbb{R})$ containing the above $\{e_j\}_{0 \le j \le N}$. For our purposes we assume that N is an even integer. For the first type of noise, we suppose that $\mathcal{Q} e_j = \lambda_j e_j$, $j = 0, \ldots, N$, for some specific choice of eigenvalues λ_j.

We then define the random variables $\tilde{f}_j^{m+\frac{1}{2}}$, describing the driving noise, as

$$\tilde{f}_j^{m+\frac{1}{2}} \stackrel{\text{def}}{=} \sqrt{\lambda_j}\, \frac{\sqrt{3}}{2} \frac{\left[\sqrt{\Delta x_{j-1}} + \sqrt{\Delta x_j}\right]}{\sqrt{\Delta t_m}\left[\Delta x_{j-1} + \Delta x_j\right]} \chi_j^{m+\frac{1}{2}},$$

where the random variables $\{\chi_j^{m+\frac{1}{2}} : m = 0, \ldots, M-1, j = 0, \ldots, N\}$ are independent Gaussian random variables $\mathcal{N}(0, 1)$. This is consistent with [36], since for the space-time white noise, all eigenvalues λ_j are equal to 1. The difference with the scheme used in [36] is that, when moving away from the origin, the effect of the noise is reduced by the factor $\sqrt{\lambda_j}$, which in the following examples will depend on the distance between x_j and 0.

We consider two types of eigenvalues $\lambda_j = \Phi_\beta(|x_j|)$, defined in terms of a function $\Phi_\beta(|x|)$, which has either an *exponential* (Gaussian-type) or a *polynomial* decay as $|x|$ grows. The positive parameter β enables us to tune the decay.

3.1.1 Example 1: Gaussian-type decay

We set

$$\Phi_\beta^{(1)}(x) = e^{-(1-\beta)x^2} \quad \text{for} \ \ \beta \in [0, 1].$$

First, observe that when $\beta \in [0, 1)$, up to some normalizing constant, $\Phi_\beta^{(1)}$ is a centered Gaussian kernel with the variance $\frac{1}{2(1-\beta)}$. Thus, when β approaches 1, it becomes more spread out. Hence, when $\beta = 1$, the kernel is a constant function $\Phi_1^{(1)} = 1$ and our

noise W becomes an approximation W_N of the space-time white noise, studied in [11,36].

We define the operator $\phi_\beta^{(1)}$ as

$$\phi_\beta^{(1)} e_j = \begin{cases} \left(\Phi_\beta^{(1)}(|x_j|)\right)^{\frac{1}{2}} e_j, & \text{for } j = 0, \dots, N, \\ 0, & \text{otherwise.} \end{cases}$$

For N even, a constant space mesh Δx_j, equal to Δx and $\beta \in [0, 1)$, $\phi_\beta^{(1)}$ is Hilbert–Schmidt from $L^2_{\mathbb{R}}(\mathbb{R})$ to $H^1_{\mathbb{R}}(\mathbb{R})$ and Radonifying from $L^2_{\mathbb{R}}(\mathbb{R})$ to $\dot{W}^{1,\infty}_{\mathbb{R}}(\mathbb{R})$. We then have $L_c = \frac{N}{2}\Delta x$, and since $\{\Phi_\beta^{(1)}(j\Delta x)\}_{j>0}$ is decreasing, we deduce

$$1 + \frac{2}{\Delta x}\int_{\Delta x}^{L_c+\Delta x} e^{-(1-\beta)x^2} dx \le \|\phi_\beta^{(1)}\|^2_{L^{0,0}_{2,\mathbb{R}}} \le 1 + \frac{2}{\Delta x}\int_0^{L_c} e^{-(1-\beta)x^2} dx.$$

As $\Delta x \to 0$ and $L_c \to \infty$, we get

$$\|\phi_\beta^{(1)}\|^2_{L^{0,0}_{2,\mathbb{R}}} \sim \frac{1}{\Delta x}\left(\frac{\pi}{1-\beta}\right)^{\frac{1}{2}}, \qquad \|\phi_\beta^{(1)}\|^2_{L^{0,1}_{2,\mathbb{R}}} \sim \frac{12}{(\Delta x)^3}\left(\frac{\pi}{1-\beta}\right)^{\frac{1}{2}},$$

and

$$m_{\phi_\beta^{(1)}} \sim \frac{12}{(\Delta x)^4}\left(\frac{\pi}{1-\beta}\right)^{\frac{1}{2}},$$

which appears in the upper estimate (2.3).

3.1.2 Example 2: polynomial decay

Fix a real number $n \ge 1$, and set

$$\Phi_\beta^{(2)}(x) = \frac{1}{\left(1+|x|\right)^{n(1-\beta)}} \quad \text{for} \quad \beta \in [0, 1].$$

(For ease of notations, n is omitted on the left-hand side.) Note that when $\beta = 0$, the decay is of the order $|x|^{-n}$ for large values of $|x|$, the fastest in this setting, and as β decreases, the noise becomes more regular. The parameter n enables us to tune this decay.

Let $\phi_\beta^{(2)}$ be the operator from $L^2_{\mathbb{R}}(\mathbb{R})$ to $H^1_{\mathbb{R}}(\mathbb{R}) \cap L^\infty_{\mathbb{R}}(\mathbb{R})$ defined by

$$\phi_\beta^{(2)}(e_j) = \begin{cases} \left(\Phi_\beta^{(2)}(x_j)\right)^{\frac{1}{2}} e_j, & \text{for } j = 0, \dots, N, \\ 0, & \text{otherwise.} \end{cases}$$

Note that if $\beta = 1$, the operator $\phi_1^{(2)}$ is the identity when restricted to span $\{e_0, \ldots, e_N\}$. This is the covariance of the projection W_N of the space-time white noise on that subspace (which was used in [11,36]). As in the previous example, we suppose that N is even, and the space mesh is uniform (thus, equal to Δx) to obtain estimates of various operator norms of $\phi_\beta^{(2)}$. We have

$$\|\phi_\beta^{(2)}\|^2_{L^{0,0}_{2,\mathbb{R}}} = \sum_{j=0}^{N} \Phi_\beta^{(2)}(x_j) = 1 + 2\sum_{j=1}^{N/2}(1 + j\Delta x)^{-n(1-\beta)}.$$

We bound the last term (noting that $\{\Phi_\beta^{(2)}(j\Delta x)\}_j$ is decreasing) as

$$\int_{\Delta x}^{L_c+\Delta x}(1+x)^{-n(1-\beta)}dx \le \Delta x \sum_{j=1}^{\frac{N}{2}}(1 + j\Delta x)^{-n(1-\beta)} \le \int_0^{L_c}(1+x)^{-n(1-\beta)}dx.$$

Hence, for a fixed L_c, as $\Delta x \to 0$, we deduce

$$\|\phi_\beta^{(2)}\|^2_{L^{0,0}_{2,\mathbb{R}}} \sim \frac{1}{\Delta x}\int_{-L_c}^{L_c}(1+|x|)^{-n(1-\beta)}dx.$$

Recalling a basic fact that the indefinite integral $I(a) \stackrel{\text{def}}{=} \int_{-\infty}^{\infty}(1+|x|)^{-a}dx$ converges if and only if $a > 1$, to the value $I(a) = \frac{2}{a-1}$, we obtain that as $\Delta x \to 0$ and $L_c \to \infty$

$$\|\phi_\beta^{(2)}\|^2_{L^{0,0}_{2,\mathbb{R}}} \sim \frac{2}{\Delta x\,(n-1-n\beta)} \quad \text{if and only if } \beta \in \Big[0, \frac{n-1}{n}\Big).$$

A similar computation for the same range $0 \le \beta < \frac{n-1}{n}$ yields

$$\|\phi_\beta^{(2)}\|^2_{L^{0,1}_{2,\mathbb{R}}} \sim \frac{24}{(\Delta x)^3\,(n-1-n\beta)},$$

and

$$m_{\phi_\beta^{(2)}} \sim \frac{24}{(\Delta x)^4\,(n-1-n\beta)}.$$

Note that for $\beta \in \big[0, 1-\frac{1}{n}\big)$, the above upper estimates for Hilbert–Schmidt and Radonifying norms are insensitive to the length L_c, however, depend on the space mesh Δx. We remark that in this range of β we have a discretization of a Q-Brownian motion.

For $\beta(n) = \frac{n-1}{n}$ we have as $\Delta x \to 0$

$$\|\phi^{(2)}_{\beta(n)}\|^2_{L^{0,0}_{2,\mathbb{R}}} \sim \frac{2}{\Delta x}\ln(L_c+1), \quad \|\phi^{(2)}_{\beta(n)}\|^2_{L^{0,1}_{2,\mathbb{R}}} \sim \frac{24}{(\Delta x)^3}\ln(L_c+1),$$
$$\text{and } m_{\phi^{(2)}_{\beta(n)}} \sim \frac{24}{(\Delta x)^4}\ln(L_c+1).$$

Finally, for $\beta \in \left(\frac{n-1}{n}, 1\right]$ we have

$$\int_{-L_c}^{L_c}(1+|x|)^{-n(1-\beta)}dx = \frac{2}{n\beta-n+1}\left[(L_c+1)^{n\beta-n+1}-1\right].$$

Hence, as $\Delta x \to 0$ and $L_c \to \infty$, when $\frac{n-1}{n} < \beta \le 1$, we obtain

$$\|\phi^{(2)}_{\beta}\|^2_{L^{0,0}_{2,\mathbb{R}}} \sim \frac{2}{\Delta x(n\beta-n+1)}\left[(L_c+1)^{n\beta-n+1}-1\right];$$

by a similar computation when $\Delta x \to 0$ and $L_c \to \infty$, we get

$$\|\phi^{(2)}_{\beta}\|^2_{L^{0,1}_{2,\mathbb{R}}} \sim \frac{24\left[(L_c+1)^{n\beta-n+1}-1\right]}{(\Delta x)^3(n\beta-n+1)},$$

and

$$m_{\phi^{(2)}_{\beta}} \sim \frac{24\left[(L_c+1)^{n\beta-n+1}-1\right]}{(\Delta x)^4(n\beta-n+1)}.$$

We note that when $\beta \in \left[1-\frac{1}{n}, 1\right]$, we no longer have the discretization of a Q-Brownian motion taking values in $L^2_{\mathbb{R}}(\mathbb{R})$.

3.2 Discrete mass and energy; upper bounds on energy

Consider the discrete mass

$$M_{\text{dis}}[u^m] \stackrel{\text{def}}{=} \frac{1}{2}\sum_{j=0}^{N}|u^m_j|^2\left(\Delta x_j + \Delta x_{j-1}\right), \tag{3.3}$$

which is conserved in our stochastic setting. Indeed, the proof of [36, Lemma 2.1] shows that the above three schemes (2.6), (2.7) and (2.8) conserve the discrete mass (3.3) at each time step: $M_{\text{dis}}[u^m] = M_{\text{dis}}[u^{m+1}]$, $m = 0, \ldots, M-1$. This proof relies only on the fact that the noise is real-valued, multiplicative, and that we use the Stratonovich integral, which gives rise to $\frac{1}{2}(u^m_j + u^{m+1}_j)$ in the scheme.

We next define the discrete energy adapted to the non-uniform mesh case

$$H_{\text{dis}}[u^m] \stackrel{\text{def}}{=} \frac{1}{2}\sum_{j=0}^{N}\left|\frac{u_{j+1}^m - u_j^m}{\Delta x_j}\right|^2 \Delta x_j - \frac{1}{4(\sigma+1)}\sum_{j=0}^{N}|u_j^m|^{2(\sigma+1)}(\Delta x_{j-1} + \Delta x_j). \tag{3.4}$$

In the deterministic case ($\epsilon = 0$), the MEC scheme (2.6) conserves the discrete energy, i.e., $H_{\text{dis}}[u^{m+1}] \equiv H_{\text{dis}}[u^m]$, which is proved by multiplying $\frac{1}{2}(\bar{u}^{m+1} - \bar{u}^m)(\Delta x_j + \Delta x_{j-1})$, summing from $j = 0$ to $j = N$ and taking the real part.

In the stochastic setting, energy is not conserved, and the following proposition provides upper estimates on the time evolution of the average of an instantaneous and a maximal discrete energy. For simplicity we consider the scheme (2.6) with a constant space and time mesh. In that case the discrete energy (3.4) simplifies to

$$H_{\text{dis}}[u^m] = \frac{1}{2}\sum_{j=0}^{N}\left|\frac{u_{j+1}^m - u_j^m}{\Delta x}\right|^2 \Delta x - \frac{1}{2(\sigma+1)}\sum_{j=0}^{N}|u_j^m|^{2(\sigma+1)}\,\Delta x.$$

Let τ_{dis}^* denote the existence time of the discrete MEC scheme.

Proposition 3.1 *Let $u_0 \in H^1$, $\phi e_j = \sqrt{\Phi_\beta(x_j)}\,e_j$ be the covariance described in terms of a function Φ_β, and $t_M < \tau_{\text{dis}}^*$ be a point of the time grid for N even and constant space and time meshes. Set $C = \frac{\sqrt{3}}{2}\big(1 + \frac{\sqrt{2e}}{\sqrt{\pi}}\big)$. Then*

$$\mathbb{E}\big(H_{\text{dis}}[u^M]\big) \le H_{\text{dis}}[u^0] + \frac{\epsilon}{2}\,M_{\text{dis}}[u^0]\frac{C}{\sqrt{\Delta x}\big(\Delta t\big)^{\frac{3}{2}}}\times \left[\sqrt{\Phi_\beta(0)} + 2\sum_{j=1}^{\frac{N}{2}}\sqrt{\Phi_\beta(j\Delta x)}\right] t_M, \tag{3.5}$$

$$\mathbb{E}\Big(\max_{0\le m\le M} H_{\text{dis}}[u^m]\Big) \le H_{\text{dis}}[u^0] + \epsilon\,M_{\text{dis}}[u^0]\frac{C}{\sqrt{\Delta x}\big(\Delta t\big)^{\frac{3}{2}}}\times \left[\sqrt{\Phi_\beta(0)} + 2\sum_{j=1}^{\frac{N}{2}}\sqrt{\Phi_\beta(j\Delta x)}\right] t_M. \tag{3.6}$$

Proof The approach is similar to that of [36, Prop. 3.2], though we include it for the sake of completeness. Multiplying the Eq. (2.6) by $-\Delta x\,(\bar{u}_j^{m+1} - \bar{u}_j^m)$, summing over $m = 0, \ldots, M-1$ and $j = 0, \ldots, N$, and using the conservation of the discrete

energy in the deterministic case, we deduce that for some real-valued random variable $R(M, N)$, which changes from one line to the next,

$$H_{\rm dis}[u^M] = H_{\rm dis}[u^0] + i\,R(M,N) + \epsilon\,\Delta x \sum_{m=0}^{M-1}\sum_{j=0}^{N}(\bar{u}_j^{m+1} - \bar{u}_j^m)\,\frac{1}{2}\big(u_j^{m+1} + u_j^m\big) f_j^{m+\frac{1}{2}}$$

$$= H_{\rm dis}[u^0] + i\,R(M,N) + \frac{\epsilon\,\Delta x}{2}\sum_{m=0}^{M-1}\sum_{j=0}^{N}\big(|u_j^{m+1}|^2 - |u_j^m|^2\big)\,f_j^{m+\frac{1}{2}} \tag{3.7}$$

$$= H_{\rm dis}[u^0] + i\,R(M,N) - \frac{\epsilon}{2\Delta t}\int_0^{t_M}\int_{\mathbb{R}} |U(s,x)|^2 W_N(ds,dx)$$

$$+ \frac{\epsilon\,\Delta x}{2}\sum_{m=0}^{M-1}\sum_{j=0}^{N}|u_j^{m+1}|^2\,f_j^{m+\frac{1}{2}}, \tag{3.8}$$

where $U(s,x)$ is the step process defined by $U(s,x) = u_j^m$ on the rectangle $[t_m, t_{m+1}) \times [x_{j-\frac{1}{2}}, x_{j+\frac{1}{2}})$. Since the discrete mass is preserved by the scheme, we have

$$\frac{\epsilon\,\Delta x}{2}\sum_{m=0}^{M-1}\sum_{j=0}^{N}|u_j^{m+1}|^2\,f_j^{m+\frac{1}{2}} \le \frac{\epsilon\,M_{\rm dis}[u^0]}{2}\sum_{m=0}^{M-1}\max_{0\le j\le N}|f_j^{m+\frac{1}{2}}|.$$

Using the definition of $f_j^{m+\frac{1}{2}}$, we deduce

$$E\Big(\max_{0\le j\le N}|f_j^{m+\frac{1}{2}}|\Big) = \frac{\sqrt{3}}{2}\,\frac{1}{\sqrt{\Delta t}\sqrt{\Delta x}}\,E\Big(\max_{0\le j\le N}\alpha_j|\chi_j^{m+\frac{1}{2}}|\Big),$$

where the random variables $\chi_j^{m+\frac{1}{2}}$ are independent standard Gaussians and $\alpha_j = \sqrt{\Phi_\beta(x_j)}$.

Next, we note the fact that if $\{G_k,\ k = 1,\ldots,n\}$ are independent standard Gaussians and $B_n = \max_{1\le k\le n}\{\gamma_k\,|G_k|\}$ for positive constants $\{\gamma_k\}$, then for $n \ge 2$

$$\mathbb{E}(B_n) \le \Big(1 + \frac{\sqrt{2e}}{\sqrt{\pi}}\Big)\sum_{k=1}^{n}\gamma_k. \tag{3.9}$$

Observe that this upper estimate is relevant in the case when the infinite series $\sum_{k\ge0}\gamma_k$ is convergent. When $\{\gamma_k\}_k$ is a constant sequence, the upper estimate (3.19), used in the proof of [36, Prop 3.2], gives a sharper upper bound. We next prove (3.9), noting

that the proof differs from the one done in [36, Prop 3.2]. For every $t > 0$ we have

$$P(B_n \le t) = \prod_{k=1}^{n} P(\gamma_k |G_k| \le t)$$
$$= \prod_{k=1}^{n} \Big[1 - P\Big(|G_1| > \frac{t}{\gamma_k}\Big)\Big] \ge 1 - \sum_{k=1}^{n} P\Big(|G_1| > \frac{t}{\gamma_k}\Big),$$

and we deduce that

$$\mathbb{E}(B_n) = \int_0^\infty P(B_n > t)\, dt \le \sum_{k=1}^{n} \Big[c_k + \int_{c_k}^{\infty} P\Big(|G_1| > \frac{t}{\gamma_k}\Big) dt\Big]$$

for any choice of positive constants $\{c_k\}_k$. Using the tail estimate

$$P(|G_1| > t) = \frac{2}{\sqrt{2\pi}} \int_t^\infty e^{-\frac{x^2}{2}} dx \le \frac{2}{\sqrt{2\pi}} \frac{1}{t} \int_t^\infty x e^{-\frac{x^2}{2}} dx = \sqrt{\frac{2}{\pi}} \frac{1}{t} e^{-\frac{t^2}{2}},$$

we obtain

$$\mathbb{E}(B_n) \le \sum_{k=1}^{n} \Big[c_k + \sqrt{\frac{2}{\pi}} \int_{c_k}^{\infty} \frac{\gamma_k}{t} e^{-\frac{1}{2}\left(\frac{t}{\gamma_k}\right)^2} dt\Big] \le \sum_{k=1}^{n} \Big[c_k + \sqrt{\frac{2}{\pi}}\, \gamma_k \int_{\frac{c_k}{\gamma_k}}^{\infty} \frac{e^{-\frac{t^2}{2}}}{t} dt\Big]$$
$$\le \sum_{k=1}^{n} \Big[c_k + \gamma_k \Big(\frac{\gamma_k}{c_k}\Big)^2 \sqrt{\frac{2}{\pi}} e^{-\frac{1}{2}\left(\frac{c_k}{\gamma_k}\right)^2}\Big].$$

Choosing $c_k \overset{\text{def}}{=} \gamma_k$, we deduce (3.9).

Keeping the real part of (3.8), we get that for $C = \frac{\sqrt{3}}{2}\left(1 + \frac{\sqrt{2e}}{\sqrt{\pi}}\right)$,

$$\mathbb{E}\big(H_{\text{dis}}[u^M]\big) \le H_{\text{dis}}[u^0] + \frac{\epsilon}{2} M_{\text{dis}}[u^0]\, M\, \frac{C}{\sqrt{\Delta t}\,\sqrt{\Delta x}} \Big[\sqrt{\Phi_\beta(0)} + 2 \sum_{j=1}^{\frac{N}{2}} \sqrt{\Phi_\beta(j\Delta x)}\Big]$$
$$\le H_{\text{dis}}[u^0] + \epsilon M_{\text{dis}}[u^0] \frac{C}{\sqrt{\Delta x}(\Delta t)^{\frac{3}{2}}} \Big[\sqrt{\Phi_\beta(0)} + 2 \sum_{j=1}^{\frac{N}{2}} \sqrt{\Phi_\beta(j\Delta x)}\Big]\, t_M.$$

This completes the proof of (3.5).

To prove (3.6), keeping the real part of (3.7) and upper estimating $|u_j^{m+1}|^2 - |u_j^m|^2$ by $|u_j^{m+1}|^2 + |u_j^m|^2$, we obtain

$$\max_{0 \le m \le M} H_{\text{dis}}[u^M] = H_{\text{dis}}[u^0] + \frac{\epsilon\, \Delta x}{2} \sum_{m=0}^{M-1} \sum_{j=0}^{N} \big(|u_j^{m+1}|^2 + |u_j^m|^2\big)\, |f_j^{m+\frac{1}{2}}|.$$

The same argument as for (3.5) concludes the proof. □

We next give explicit bounds (3.5)–(3.6) for the two examples described above.

Example 1 From $\Phi_\beta^{(1)}(x) = e^{-(1-\beta)x^2}$, we have $\Phi_\beta^{(1)}(0) = 1$, and for $\beta \in [0, 1)$

$$\sum_{j=1}^{\frac{N}{2}} \sqrt{\Phi_\beta^{(1)}(j\Delta x)} \le \frac{1}{\Delta x} \int_0^{L_c} e^{-\frac{(1-\beta)}{2}x^2}\, dx \le \frac{1}{\Delta x}\, \frac{\sqrt{2\pi}}{2}\, \frac{1}{\sqrt{1-\beta}}.$$

Thus,

$$\mathbb{E}\big(H_{\text{dis}}[u^M]\big) \le H_{\text{dis}}[u^0] + \frac{\epsilon}{2}\, M_{\text{dis}}[u^0]\, \frac{C}{\sqrt{\Delta x}\,(\Delta t)^{\frac{3}{2}}} \Big[1 + \frac{\sqrt{2\pi}}{\Delta x\, \sqrt{1-\beta}}\Big]\, t_M;$$

a similar bound holds for (3.6).

Example 2 From $\Phi_\beta^{(2)}(x) = (1 + |x|)^{-n(1-\beta)}$, we have $\Phi_\beta^{(2)}(0) = 1$ and

$$\sum_{j=1}^{\frac{N}{2}} \sqrt{\Phi_\beta^{(1)}(j\Delta x)} \le \frac{1}{\Delta x} \int_0^{L_c} (1+x)^{-\frac{n(1-\beta)}{2}}\, dx.$$

If $\beta \in \big[0, 1 - \frac{2}{n}\big)$, we deduce that

$$\sum_{j=1}^{\frac{N}{2}} \sqrt{\Phi_\beta^{(2)}(j\Delta x)} \le \frac{2}{\big[n(1-\beta) - 2\big]\Delta x}.$$

If $\beta \in \big[1 - \frac{2}{n}, 1\big)$, then the above sum also depends on L_c, more precisely,

$$\sum_{j=1}^{\frac{N}{2}} \sqrt{\Phi_\beta^{(2)}(j\Delta x)} \le \frac{\ln(L_c)}{\sqrt{\Delta x}} \quad \text{for} \quad \beta = 1 - \frac{2}{n},$$

$$\sum_{j=1}^{\frac{N}{2}} \sqrt{\Phi_\beta^{(2)}(j\Delta x)} \le \frac{2}{2 - n(1-\beta)} \Big[L_c^{1-\frac{n(1-\beta)}{2}} - 1\Big]\, \frac{1}{\Delta x} \quad \text{for} \quad \beta \in \big(1 - \frac{2}{n}, 1\big).$$

Substituting the above into (3.5) or (3.6), we obtain the bounds in Example 2.

From the above analysis, we find that the upper bounds for the discrete energy can depend on parameters Δx, L_c, Δt and ϵ. We will next investigate this dependence numerically.

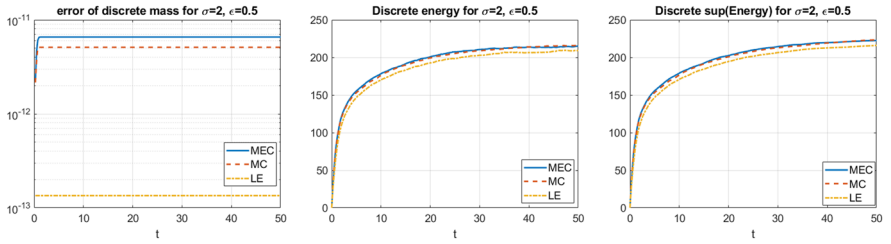

Fig. 1 Accuracy of the three schemes with the noise in Example 2, $n = 2$. The L^2-critical case ($\sigma = 2$) with $u_0 = 0.9Q$, $\beta = 0.5$, $\epsilon = 0.5$, $L_c = 20$, $\Delta x = 0.1$ and $\Delta t = 0.01$. The left plot is the error $\mathcal{E}^m[M]$ defined in (3.10) in computation of the discrete mass for all three schemes. The growth of average instantaneous energy (middle) and maximum energy (right) for different numerical schemes

3.3 Numerical tracking of discrete energy

We first show the accuracy of all three schemes in discrete mass and energy computations for the Q-Brownian driving noise. We take initial data of type $u_0 = A\,Q$, where Q is the ground state from (1.5), and obtain the error in computing the discrete mass (since it is supposed to be conserved) and then track the growth of the discrete energy (both instantaneous and maximum up to some given time t).

In Fig. 1 we show the accuracy of our computations in the L^2-critical case ($\sigma = 2$) for the initial data $u_0 = 0.9\,Q$. The left graph shows the accuracy of all three schemes in computing the discrete mass. The error is defined as

$$\mathcal{E}^m[M] \stackrel{\text{def}}{=} \max_m \left\{M_{\text{dis}}[u^m]\right\} - \min_m \left\{M_{\text{dis}}[u^m]\right\}, \tag{3.10}$$

and is on the order of $10^{-13}, \ldots, 10^{-11}$, with the linear extrapolation (LE) scheme outperforming slightly the other two schemes (it does not accumulate any error from solving a nonlinear system in the fixed point iteration as the other two schemes). The middle and right subplots show the growth and leveling off of the expected value of energy in Example 2 (we omit Example 1 as it is similar and has faster decay), the instantaneous energy (in the middle) and the average of sup energy (on the right). The average here was computed out of 100 runs. For (a large number of) multiple runs, it is significantly faster to use the LE scheme.

We next investigate the time evolution of energy. We consider both L^2-critical and supercritical cases, and study solutions on the time interval $0 \le t \le 100$. For that we take $u_0 = AQ$ with $A = 0.9$ in the L^2-critical ($\sigma = 2$) case, and $A = 0.8$ in the L^2-supercritical ($\sigma = 3$) case. The reason for a smaller coefficient in the supercritical case is to ensure that solutions exist on this time interval (see more about that at the end of Sect. 5).

Figure 2 tracks the time evolution of the discrete energy in Example 1 (Gaussian-type decay of eigenvalues) and its dependence on L_c, Δx and Δt. We note that there is leveling off in the dependence on L_c and Δt, and there is an inverse dependence on Δx. In Fig. 3 we track the dependence of energy on correlation β and noise strength ϵ in this example.

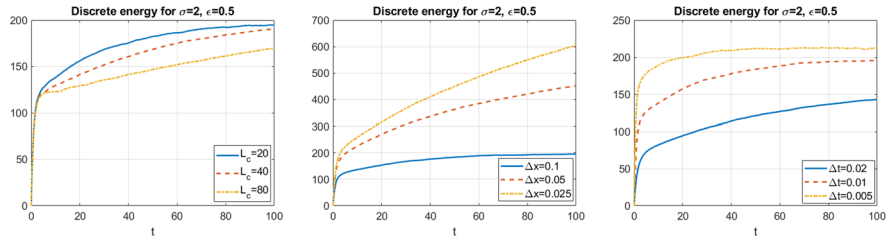

Fig. 2 Time evolution of energy and its dependence on parameters L_c (left), Δx (middle) and Δt (right), the noise is Gaussian-type decay kernel (Example 1) with $\beta = 0.5$ and $\epsilon = 0.5$

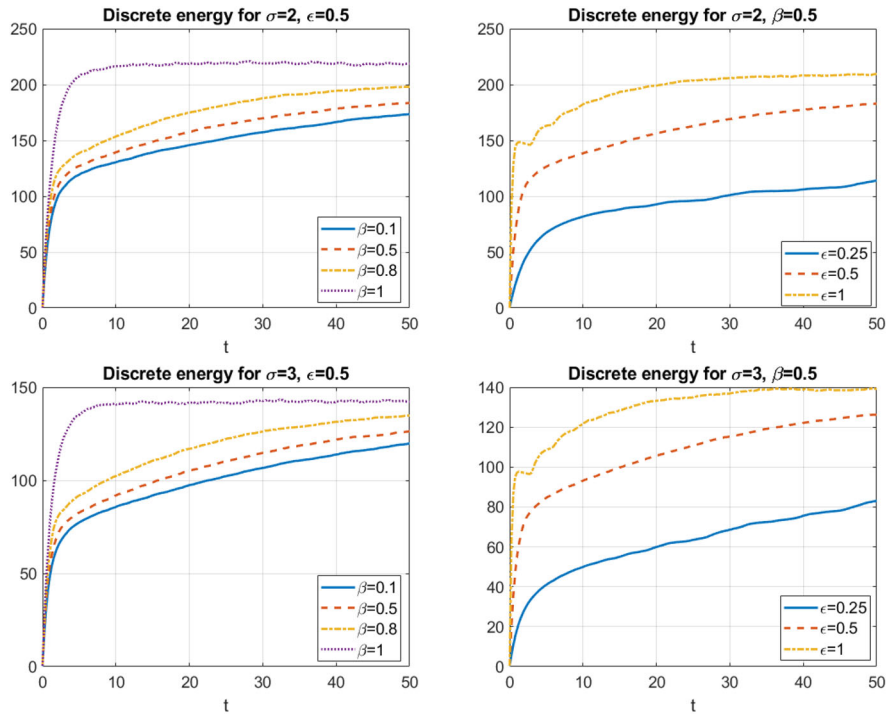

Fig. 3 The growth of energy for different values of β (left) and ϵ (right) in Example 1 (Gaussian decay) with $L_c = 20$, $\Delta x = 0.1$ and $\Delta t = 0.01$. Comparison is given in both L^2-critical and supercritical cases for the same $\epsilon = 0.5$ on the left two plots, and for the same $\beta = 0.5$ on the right two plots

In Figs. 4, 5 and 6 we study the time evolution of energy when the covariance of the driving noise has a polynomial decay (Example 2). In Fig. 4 we show how energy depends on L_c, Δx and Δt (note the dependence on Δx).

In Fig. 5 the dependence on the correlation parameter β and the strength of the noise ϵ is shown, for $n = 2$ (energy levels off, in some cases eventually; reaching the horizontal asymptote faster for larger β, when the kernel is less spread out, or for larger ϵ, when the strength of the noise is higher).

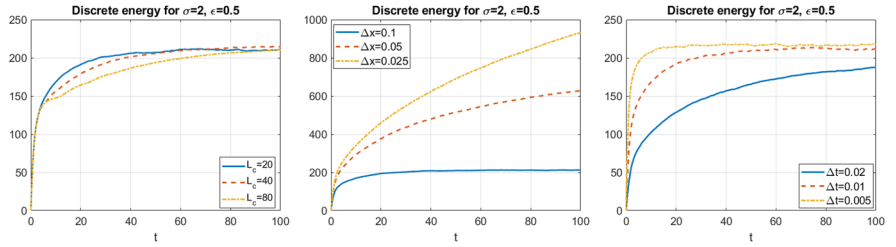

Fig. 4 Time evolution of energy and its dependence on parameters L_c (left), Δx (middle) and Δt (right) in Example 2 (polynomial decay) with $n = 2$, $\beta = 0.5$ and $\epsilon = 0.5$

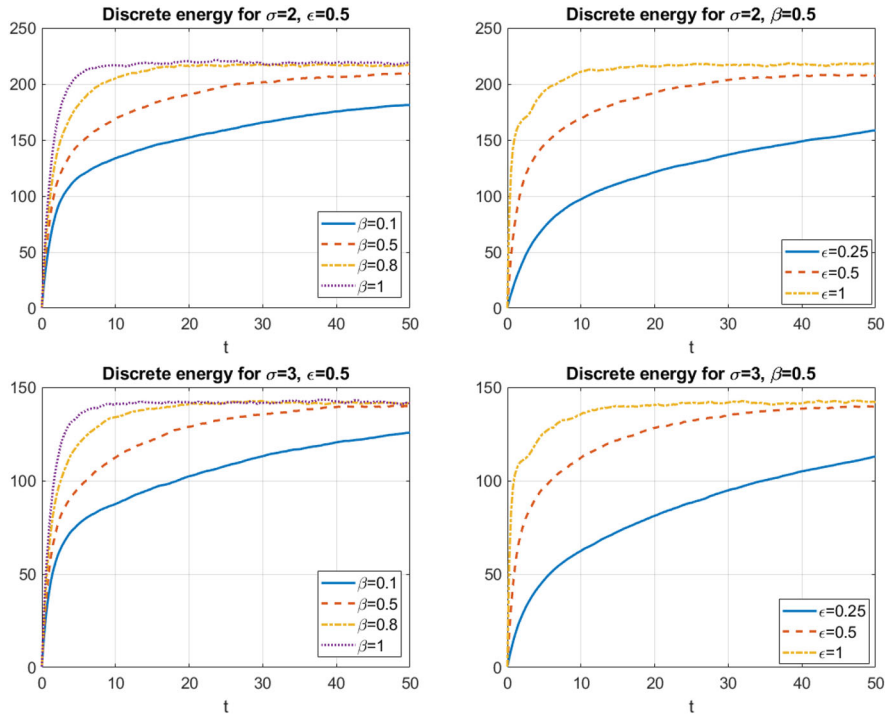

Fig. 5 The growth of energy for different values of β (left) and ϵ (right) in Example 2 (polynomial decay) with $n = 2$, $L_c = 20$, $\Delta x = 0.1$ and $\Delta t = 0.01$. Comparison is given in both L^2-critical and supercritical cases for the same $\epsilon = 0.5$ on the left two plots, and for the same $\beta = 0.5$ on the right two plots

In Fig. 6 we take $n = 4$ and vary the correlation parameter β, noting that for larger β the energy gets slightly larger and stabilizes faster, and that there is almost no dependence on L_c.

We summarize that in both Example 1 and 2, the energy grows sharply in the beginning, then slows down in its growth and levels off: the larger the strength of the noise ϵ is, or the closer it is to the space-time white noise (in other words, the more irregular the noise becomes), or the smaller the time step is, then the faster the discrete energy levels off. As in [36], it seems to be very sensitive to the space mesh

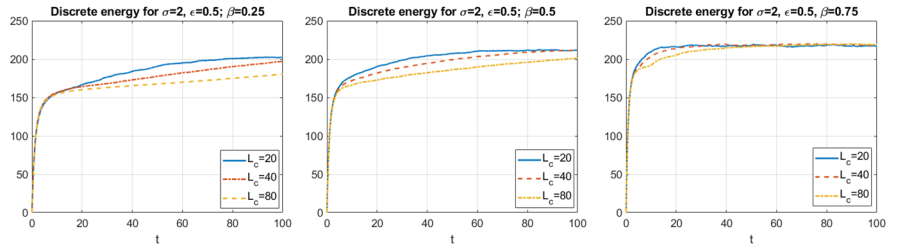

Fig. 6 The growth of energy in Example 2 (polynomial decay) with $n = 4$, for different values of L_c with $\beta = 0.25$ (left), $\beta = 0.5$ (middle) and $\beta = 0.75$ (right)

size Δx, but not sensitive to the length of the computational interval L_c. Furthermore, the numerical growth of energy is smaller than the theoretical upper bounds.

4 Stochastic perturbation driven by a homogeneous Wiener process

In this section we discuss another classical way to smooth the space-time white noise in the space variable. As in the previous section, the noise will be white in time and colored in space. However, it will not be an $L^2_{\mathbb{R}}(\mathbb{R})$-valued process and, as in [11,36], we will have to consider a partial sum of an infinite diverging series.

4.1 Description of the driving noise

Let $\mathcal{D}(\mathbb{R}^2)$ be the set of C^∞-functions with compact support. Let $\tilde{W} = \{W(\phi); \phi \in \mathcal{D}(\mathbb{R}^2)\}$ be an $L^2(\Omega)$-valued centered Gaussian process with covariance defined by

$$\mathbb{E}\big(\tilde{W}(\phi)\,\tilde{W}(\psi)\big) = J(\phi,\psi) \stackrel{\text{def}}{=} \int_0^\infty ds \int_{\mathbb{R}} dx \int_{\mathbb{R}} \phi(s,x)\tilde{\Phi}(|x-y|)\psi(s,y)\,dy$$
$$\text{for } \phi, \psi \in \mathcal{D}(\mathbb{R}^2).$$

We assume that the function $\tilde{\Phi}$ (which may be defined almost everywhere) is the density of a measure, which is the Fourier transform of a tempered symmetric measure μ (referred to as its spectral measure). Indeed, this requirement is a necessary and sufficient condition for $J(\cdot,\cdot)$ to be non-negative definite and to define a covariance structure (for more details see [6, pp. 5, 6]). To stress the difference with examples in the previous Sect. 3 we denote the covariance kernel by $\tilde{\Phi}$.

We are interested in two cases, which we call Examples 3 and 4.

4.1.1 Example 3: Riesz kernel

Let $\beta \in (0,1)$, and recall the Riesz kernel, defined by

$$R_\beta(x) = |x|^{-\beta} \text{ for } x \neq 0, \quad \text{and } R_\beta(0) = +\infty.$$

In order to make sure that when $\beta \to 1$, the corresponding homogeneous noise approaches the space time white noise, as in Examples 1 and 2 considered in Sect. 3, we modify the Riesz kernel, multiplying it by the constant $\frac{(1-\beta)(2-\beta)}{2}$, to read

$$\tilde{\Phi}_\beta^{(3)}(x) = \frac{(1-\beta)(2-\beta)}{2}\,|x|^{-\beta} \text{ for } x \neq 0, \quad \text{and } \tilde{\Phi}_\beta^{(3)}(0) = +\infty.$$

This comes down to changing the coefficient ϵ by another one depending on β. The Fourier transform of R_β is the function $\nu_\beta(x) = C(\beta)R_{1-\beta}(x)$ for some positive constant $C(\beta)$. Note that it is symmetric and is the density of a measure, which is a tempered distribution. The Riesz kernel $|x|^{-\beta}$ has a singularity at the origin.

As $\beta \to 1$, we get the limiting case $\beta = 1$ of the modified kernel $\tilde{\Phi}_1^{(3)}$, which corresponds to the space-time white noise (see (4.3) and discussion afterwards).

4.1.2 Example 4: exponential kernel

For $\beta > 0$ we define $\tilde{\Phi}_\beta^{(4)}$ by

$$\tilde{\Phi}_\beta^{(4)}(x) = e^{-\beta|x|}.$$

For large values of $|x|$, the decay of $\tilde{\Phi}_\beta^{(4)}(x)$ is exponential, hence, faster than that of the Riesz kernel $|x|^{-\beta}$ from Example 3, which is polynomial. The Fourier transform of $\tilde{\Phi}_\beta^{(4)}$ is the function $G(x) = \frac{2\beta}{\beta^2+4\pi^2x^2}$; note that the symmetric measure $G(x)dx$ is a tempered distribution.

4.1.3 Covariance matrices

We do not deal with a diagonal matrix anymore as in Examples 1 and 2; instead we consider the covariance matrix

$$\Gamma(j,k) \stackrel{\text{def}}{=} \int_{\mathbb{R}} dx \int_{\mathbb{R}} \tilde{e}_j(x)\,\tilde{\Phi}(|x-y|)\,\tilde{e}_k(y)\,dy, \quad j,k = 0,\ldots,N, \tag{4.1}$$

for some choice of orthonormal vectors $\{\tilde{e}_j\}_{0\le j\le N}$. The assumptions made on the existence of the spectral measure of $\tilde{\Phi}(x)dx$ ensure that the symmetric $(N+1)\times(N+1)$-matrix Γ is positive definite. Let ϕ be the operator defined by $\phi\,\tilde{e}_j(x) = \int_{\mathbb{R}} \tilde{e}_j(y) f(|x-y|)dy$, where $\tilde{\Phi}(x-y) = \int_{\mathbb{R}} f(|x-z|) f(|z-y|)dz = \int_{\mathbb{R}} f(|x-y-z|) f(|z|)dz$. To make numerical computations easier, for this type of noise in Examples 3 and 4 we use indicator functions $\tilde{e}_j$. Indeed, thanks to the regularization effect of the convolution used in the definition of ϕ, the regularity of the function $\tilde{\Phi}$ makes it possible to have an $H^1_{\mathbb{R}}(\mathbb{R})$-valued function $\phi\,\tilde{e}_j$ when $\tilde{e}_j$ is an indicator function.

Recalling that $x_{j+\frac{1}{2}} = \frac{1}{2}(x_j + x_{j+1})$, we define the functions $\{\tilde{e}_j\}_{0\le j\le N}$ as

$$\tilde{e}_j = \frac{\sqrt{2}}{\sqrt{\Delta x_{j-1} + \Delta x_j}} 1_{[x_{j-\frac{1}{2}}, x_{j+\frac{1}{2}}]}, \quad j = 1, \dots, N-1,$$
$$\tilde{e}_0 = \frac{\sqrt{2}}{\sqrt{\Delta x_0}} 1_{[x_0, x_{\frac{1}{2}}]}, \quad \tilde{e}_N = \frac{\sqrt{2}}{\sqrt{\Delta x_{N-1}}} 1_{[x_{N-\frac{1}{2}}, x_N]}.$$

Note that $\{\tilde{e}_j\}_{0\le j\le N}$ are orthonormal functions in $L^2_{\mathbb{R}}(\mathbb{R})$. We will now write the covariance matrices explicitly for each of the above two examples. In order to produce the covariance matrix that will be used to define the driving perturbation in our simulations, we renormalize Γ to $\tilde{\Gamma}$ defined by

$$\tilde{\Gamma}(j,k) = \frac{2}{\sqrt{\Delta x_{j-1} + \Delta x_j}\sqrt{\Delta x_{k-1} + \Delta x_k}} \Gamma(j,k), \quad j,k = 0, \dots, N. \quad (4.2)$$

Example 3 For the Riesz kernel the renormalized covariance matrix $\tilde{\Gamma}^{(3)}_\beta$ is defined for $j,k = 0,\dots,N$ by

$$\tilde{\Gamma}^{(3)}_\beta(j,k) = 2\left(\frac{\left|x_{k+\frac{1}{2}} - x_{j-\frac{1}{2}}\right|^{2-\beta} + \left|x_{k-\frac{1}{2}} - x_{j+\frac{1}{2}}\right|^{2-\beta} - \left|x_{k+\frac{1}{2}} - x_{j+\frac{1}{2}}\right|^{2-\beta} - \left|x_{k-\frac{1}{2}} - x_{j-\frac{1}{2}}\right|^{2-\beta}}{(\Delta x_{j-1} + \Delta x_j)(\Delta x_{k-1} + \Delta x_k)}\right). \quad (4.3)$$

Note that $\tilde{\Gamma}^{(3)}_\beta$ is positive definite. Furthermore, if $\beta = 1$, it is easy to see that $\tilde{\Gamma}^{(3)}_1(k,k) = \frac{2}{\Delta x_{k-1}+\Delta x_k}$ and $\tilde{\Gamma}^{(3)}_1(j,k) = 0$ for $j,k = 0,\dots,N$, $j \ne k$. This is the renormalized version of the covariance matrix of the space-time white noise used in [36].

Example 4 For the exponential kernel, the renormalized covariance matrix $\tilde{\Gamma}^{(4)}_\beta$ is defined by

$$\tilde{\Gamma}^{(4)}_\beta(k,k) = \frac{4}{(\Delta x_{k-1} + \Delta x_k)^2}\left[\frac{\Delta x_{k-1} + \Delta x_k}{\beta} - \frac{2}{\beta^2}\left(1 - e^{-\frac{\beta}{2}(\Delta x_{k-1} + \Delta x_k)}\right)\right]$$

for $k = 0,\dots,N$, and

$$\tilde{\Gamma}^{(4)}_\beta(j,k) = 4\,\frac{e^{-\beta\left|x_{k-\frac{1}{2}} - x_{j+\frac{1}{2}}\right|} + e^{-\beta\left|x_{k+\frac{1}{2}} - x_{j-\frac{1}{2}}\right|} - e^{-\beta\left|x_{k-\frac{1}{2}} - x_{j-\frac{1}{2}}\right|} - e^{-\beta\left|x_{k+\frac{1}{2}} - x_{j+\frac{1}{2}}\right|}}{\beta^2\left(\Delta x_{j-1} + \Delta x_j\right)\left(\Delta x_{k-1} + \Delta x_k\right)}$$

for $j \ne k$, $j,k = 0,\dots,N$.

4.2 Covariance matrix computation, bounds on discrete energy

As in Sect. 3, we use mass-conservative schemes. However, the functions $\{\tilde{e}_j\}_{0\le j\le N}$ do not give rise to a diagonal covariance matrix. This is due to the fact that the noise correlation involves a convolution, which has long-range effects and gives rise to a full matrix.

In order to simulate a centered Gaussian $(N+1)$-dimensional vector with covariance matrix $\tilde{\Gamma}$, we use the Cholesky decomposition of $\tilde{\Gamma}$. This is possible in Examples 3 and 4, since the covariance matrices are positive-definite. More precisely, we find a lower triangular matrix A such that $\tilde{\Gamma} = AA^*$, where A^* denotes the transposed matrix of A. Therefore, if $Y = (Y_0, \dots, Y_N)$ denotes an $(N+1)$-dimensional Gaussian vector with independent components, which are standard Gaussian (i.e., $\mathcal{N}(0,1)$) random variables, the covariance matrix of Y is Id. Let $\mathcal{A}$ be the linear operator on $\mathbb{R}^{N+1}$, whose matrix in the canonical basis is A. Then $X \overset{\text{def}}{=} \mathcal{A}Y$ is a centered Gaussian random vector with covariance matrix $\tilde{\Gamma}$. We then have to produce a vector $u^{m+1} \overset{\text{def}}{=} (u_0^{m+1}, \dots, u_N^{m+1})$ in terms of the vector $u^m = (u_0^m, \dots, u_N^m)$ (and can no longer define an isolated component u_j^{m+1} in terms of u_j^m for some $j = 0, \dots, N$).

Let $\chi^{m+\frac{1}{2}} \overset{\text{def}}{=} (\chi_0^{m+\frac{1}{2}}, \dots, \chi_N^{m+\frac{1}{2}})$ denote a Gaussian vector whose components are independent $\mathcal{N}(0,1)$ random variables. Then set for $j = 0, \dots, N$

$$\tilde{f}^{m+\frac{1}{2}} = \frac{1}{\sqrt{\Delta t_m}}\,\mathcal{A}\chi^{m+\frac{1}{2}} \quad \text{and} \quad f_j^{m+\frac{1}{2}} = \frac{u_j^m + u_j^{m+1}}{2}\,\tilde{f}_j^{m+\frac{1}{2}}. \tag{4.4}$$

With this definition of the vector $\{f_j^{m+\frac{1}{2}}\}_j$, we define analogs of the three schemes in (2.6)–(2.8).

4.2.1 Upper bounds on discrete energy

We remind that the discrete mass $M_{\text{dis}}[u]$ defined in (3.3) is conserved, due to the fact that the noise is real-valued and the factor $\frac{1}{2}(u_j^m + u_j^{m+1})$ used to define $f_j^{m+\frac{1}{2}}$ corresponds to the discretization of the Stratonovich integral. We next prove an upper bound of the average of the instantaneous and maximal discrete energy.

Proposition 4.1 *Let u^m be the solution of the MEC scheme (2.6) with a constant time and space mesh, for a random perturbation defined by (4.2). Suppose that $\sup_{0\le k\le N} \tilde{\Gamma}(k,k) \le \delta^2$ for some positive constant δ^2. Let τ^* denote the random existence time of this scheme. Then for every time $t_M < \tau^*$ on the time grid, we have that for $\Delta x \in (0,1)$*

$$\mathbb{E}\big(H_{\rm dis}[u^M]\big) \le H_{\rm dis}[u^0] + \frac{\epsilon\, M_{\rm dis}[u^0]}{\sqrt{2}\,(\Delta t)^{\frac{3}{2}}}\,\delta\,\sqrt{\ln(4\,L_c) + |\ln(\Delta x)|}\;t_M, \quad (4.5)$$

$$\mathbb{E}\Big(\max_{0\le m\le M} H_{\rm dis}[u^m]\Big) \le H_{\rm dis}[u^0] + \frac{\sqrt{2}\,\epsilon\, M_{\rm dis}[u^0]}{(\Delta t)^{\frac{3}{2}}}\,\delta\,\sqrt{\ln(4\,L_c) + |\ln(\Delta x)|}\;t_M. \quad (4.6)$$

Proof We proceed as in the proof of Proposition 3.1. Using (3.8), we see that we need to find an upper estimate of $\mathbb{E}\big(\max_{0\le k\le N}|X_k^{m+\frac{1}{2}}|\big)$, where $\{X_j^{m+\frac{1}{2}}\}_j$ is a centered Gaussian vector with a covariance matrix Γ. Note that for every $k = 0, \dots, N$, $\mathrm{Var}(X_k^{m+\frac{1}{2}}) \le \delta^2$, so that for every $\lambda > 0$,

$$\mathbb{E}\Big(e^{\lambda\,|X_k^{m+\frac{1}{2}}|}\Big) = \frac{2}{\delta\sqrt{2\pi}}\int_0^\infty e^{-\frac{x^2}{2\delta^2}+\lambda x}\,dx \le 2e^{\frac{\lambda^2\delta^2}{2}}.$$

The next argument is a slight extension of the one used in the proof of [36, Prop 3.2], where the random variables $X_j^{m+\frac{1}{2}}$ were standard Gaussians; it is based on the Pisier lemma (see, e.g., [28, Lemma 10.1]). We have

$$\mathbb{E}\Big(\max_{0\le j\le N}\big|X_j^{m+\frac{1}{2}}\big|\Big) \le \delta\,\sqrt{2\ln\big[2\,(N+1)\big]}. \quad (4.7)$$

We include its short proof for completeness. For any $\lambda > 0$, using the Jensen inequality and the fact that $x \mapsto e^{\lambda x}$ is increasing, we obtain

$$\begin{aligned}\exp\Big(\lambda\mathbb{E}\big[\max_{0\le k\le N}|X_k^{m+\frac{1}{2}}|\big]\Big) &\le \mathbb{E}\Big(\exp\Big[\lambda\max_{0\le k\le N}\big|X_k^{m+\frac{1}{2}}|\Big]\Big)\\ &\le \mathbb{E}\Big(\max_{0\le k\le N}\exp\big(\lambda|X_k^{m+\frac{1}{2}}|\big)\Big)\\ &\le \sum_{k=0}^{N}\mathbb{E}\Big(e^{\lambda\left|X_k^{m+\frac{1}{2}}\right|}\Big) \le 2\,(N+1)e^{\frac{\lambda^2\delta^2}{2}}.\end{aligned}$$

Taking logarithms, we deduce

$$\mathbb{E}\Big(\max_{0\le k\le N}|X_k^{m+\frac{1}{2}}|\Big) \le \frac{1}{\lambda}\ln\Big(2\,(N+1)e^{\frac{\lambda^2\delta^2}{2}}\Big) = \frac{\ln\big[2\,(N+1)\big]}{\lambda} + \frac{\lambda\,\delta^2}{2},$$

for every $\lambda > 0$. Choosing $\lambda = \frac{\sqrt{2\ln[2\,(N+1)]}}{\delta}$ for $N \ge 1$, concludes the proof of (4.7).

Therefore, as in the proof of Proposition 3.1, we have

$$\mathbb{E}\big(H_{\rm dis}[u^M]\big) \le H_{\rm dis}[u^0] + \sum_{m=0}^{M-1}\frac{\epsilon}{2}M_{\rm dis}[u^0]\frac{1}{\sqrt{\Delta t}\sqrt{\Delta x}}\delta\,\sqrt{2\ln\big[2\,(N+1)\big]}.$$

This concludes the proof of (4.5). The inequality (4.6) is obtained in a similar manner. □

We next compute the upper bounds of the average discrete energy in the two examples of homogeneous noise.

Example 3 The definition of $\tilde{\Gamma}_\beta^{(3)}$ for a constant space mesh Δx implies that $\tilde{\Gamma}_\beta^{(3)}(k,k) = \big(\Delta x\big)^{-\beta}$ for $k = 0, \ldots, N$. Therefore, the assumptions of Proposition 4.1 are satisfied with $\delta_\beta^{(3)} = \big(\Delta x\big)^{-\frac{\beta}{2}}$, and for $\Delta x \in (0,1)$ the estimate (4.5) becomes

$$\mathbb{E}\big(H_{\rm dis}[u^M]\big) \le \; H_{\rm dis}[u^0] + \frac{\epsilon M_{\rm dis}[u^0]}{\sqrt{2}\,(\Delta t)^{\frac{3}{2}}(\Delta x)^{\frac{\beta}{2}}}\sqrt{\ln(2\,L_c) + |\ln(\Delta x)|}\;t_M.$$

Example 4 The definition of $\tilde{\Gamma}_\beta^{(4)}$ for a constant space mesh Δx implies that for $k = 0, \ldots, N$

$$\tilde{\Gamma}_\beta^{(4)}(k,k) = \frac{1}{(\Delta x)^2}\left[\frac{2\,\Delta x}{\beta} - \frac{2}{\beta^2}\big(1 - e^{-\beta\,\Delta x}\big)\right],$$

which, from Taylor expansion, is lower and upper bounded as

$$1 - \frac{\beta\Delta x}{3} \le \tilde{\Gamma}_\beta^{(4)}(k,k) \le 1 - \frac{\beta\Delta x}{3} + \frac{(\beta\,\Delta x)^2}{12} \le 1.$$

Therefore, the assumptions of Proposition 4.1 are satisfied with $\delta_\beta^{(4)} = \Big(1 - \frac{\beta\Delta x}{3} + \frac{(\beta\,\Delta x)^2}{12}\Big)^{\frac{1}{2}}$, and the upper estimate (4.5) becomes

$$\begin{aligned}\mathbb{E}\big(H_{\rm dis}[u^M]\big) \le \; & H_{\rm dis}[u^0] \\ & + \frac{\epsilon M_{\rm dis}[u^0]}{2\,(\Delta t)^{\frac{3}{2}}}\Big(1 - \frac{\beta\Delta x}{3} + \frac{(\beta\,\Delta x)^2}{12}\Big)^{\frac{1}{2}}\sqrt{2\big[\ln(2\,L_c) + |\ln(\Delta x)|\big]}\,t_M \\ \le \; & H_{\rm dis}[u^0] + \frac{\epsilon M_{\rm dis}[u^0]}{\sqrt{2}\,(\Delta t)^{\frac{3}{2}}}\sqrt{\ln(2\,L_c) + |\ln(\Delta x)|}\,t_M.\end{aligned}$$

4.3 Numerical tracking of discrete energy

To check the accuracy of our three schemes for this homogeneous type of noise, we show the error $\mathcal{E}^m[M]$ defined in (3.10) in the computation of the discrete mass in the left subplot of Fig. 7, and the growth of the discrete energy in the middle and right subplots of Fig. 7. There we consider the L^2-critical case and take $u_0 = 0.9Q$ as the initial condition with the noise from Example 3 (Riesz kernel) with $\beta = 0.5$ and noise strength $\epsilon = 0.5$. Our other computational parameters are the same as in Fig. 1: $L_c = 20$, $\Delta x = 0.1$, $\Delta t = 0.01$. One can see that the error in mass is

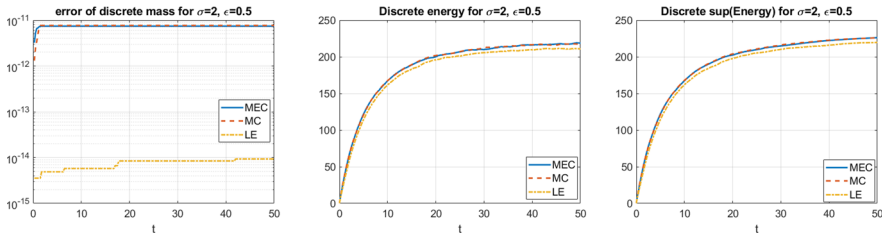

Fig. 7 Accuracy of the three schemes with the noise in Example 3 (Riesz kernel). The L^2-critical case ($\sigma = 2$) with $u_0 = 0.9Q$, $\beta = 0.5$, $\epsilon = 0.5$, $L_c = 20$, $\Delta x = 0.1$ and $\Delta t = 0.01$. The left plot is the error $\mathcal{E}^m[M]$ (3.10) in computation of the discrete mass for three schemes. The growth of average (instantaneous) energy (middle) and max energy (right) from different numerical schemes

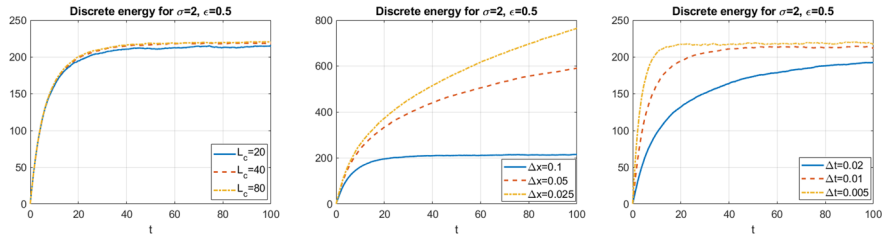

Fig. 8 Time evolution of energy and its dependence on parameters L_c (left), Δx (middle) and Δt (right) in Example 3 (Riesz kernel) in the L^2-critical case with $n = 2$, $\beta = 0.5$ and $\epsilon = 0.5$

similar to the Example 2 in Fig. 1, as well as the average energy (both instantaneous and maximal as defined by the left-hand sides of (4.5) and (4.6), respectively) grow and level off similarly. The LE scheme is slightly under-performing (probably due to slower catching up, since there is no nonlinear correction used in the LE scheme). Changing various parameters, we find similar behavior in accuracy, concluding that for all types of driving noises considered, our numerical simulations are sufficiently accurate.

We next study how the energy is affected by the spatially homogeneous noise from Examples 3 and 4 (see Figs. 8, 9, 10, 11 and 12). First, we note that the discrete energy does not depend on the length of the computational domain L_c, see left subplots in Figs. 8 and 10. In Example 3 (with the Riesz kernel singular at the origin), we observe a clear dependence on the spatial mesh size Δx: the smaller the size, the faster the growth of the energy is; see the middle subplot in Fig. 8. In Example 4 (with a more regular kernel having an exponential decay) there is almost no dependence on Δx; see middle subplot in Fig. 10. The right subplots in Figs. 8 and 10 show the dependence on the time step size Δt: in Fig. 8 (Riesz kernel) it has some influence on how fast the energy grows initially, however, eventually it starts leveling off and approaching a horizontal asymptote; in Fig. 10 (Example 4), where the kernel has an exponential decay, it takes a longer time to reach the horizontal asymptote, especially for larger time steps (e.g. for $\Delta t = 0.02$ in the right subplot in Fig. 10). In these computations we tracked the energy on the time interval $(0, 100)$ for comparison purposes, it is possible to obtain longer time tracking (see, for example, Fig. 12, however, it does take longer

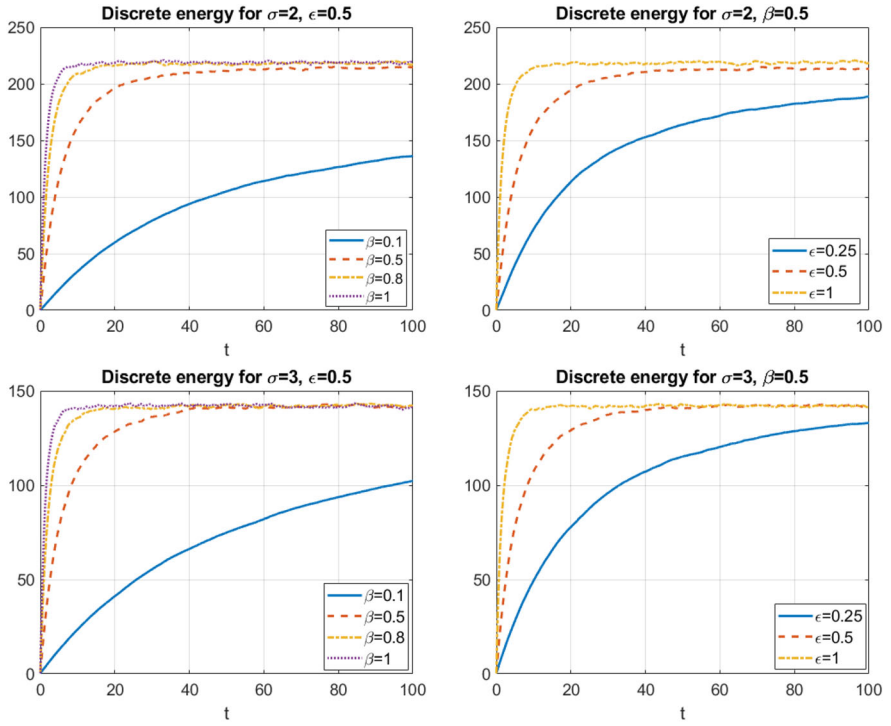

Fig. 9 The growth of energy for different values of β (left) and ϵ (right) in Example 3 (Riesz kernel) with $L_c = 20$, $\Delta x = 0.1$ and $\Delta t = 0.01$. Comparison is given in both L^2-critical and supercritical cases for the same $\epsilon = 0.5$ on the left two plots, and for the same $\beta = 0.5$ on the right two plots

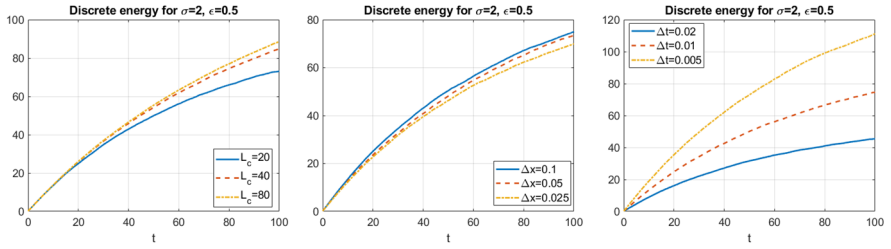

Fig. 10 Time evolution of energy and its dependence on parameters L_c (left), Δx (middle) and Δt (right) in Example 4 (exponential kernel) in the L^2-critical case with $n = 2$, $\beta = 0.5$ and $\epsilon = 0.5$

computational time to track the energy growth, since it requires at least 100 trials to run in each particular value of a parameter to approximate the expected values).

We next track the influence of the noise strength ϵ and the correlation parameter β on the energy growth in Examples 3 and 4. Figure 9 shows that the energy first increases, and then reaches the horizontal asymptote. The leveling off is clearly seen in Fig. 9, Example 3 (Riesz kernel). This is similar to what we observed for the SNLS with space-time driving Brownian motion in [36] corresponding to $\beta = 1$ in the first three examples. It does not seem to behave similarly in Example 4, see Fig. 11,

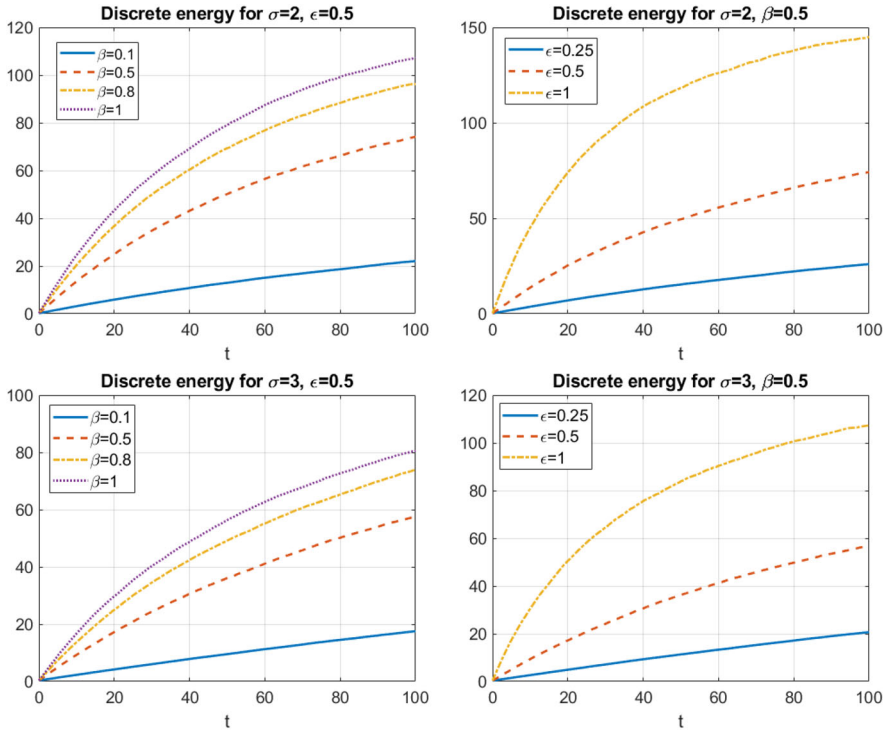

Fig. 11 The growth of energy for different values of β (left) and ϵ (right) in Example 4 (exponential kernel) with $L_c = 20$, $\Delta x = 0.1$ and $\Delta t = 0.01$. Comparison is given in both L^2-critical and supercritical cases for the same $\epsilon = 0.5$ on the left two plots, and for the same $\beta = 0.5$ on the right two plots

however, if we track the energy for longer times, for example, to time $t = 200$—see Fig. 12, the energy starts leveling off. Note that in this Example 4, the parameter β can have values beyond 1. Larger values of β represent more irregular noise, and we note that in that case the energy approaches the horizontal asymptote faster; see Fig. 12.

To summarize, the stronger or more irregular the noise is (that is, the larger ϵ or β is), the faster the convergence to the horizontal asymptote becomes. We also observe that regardless of the noise strength, the values of the discrete energy converge to the same horizontal asymptote; we also observed this in [36] for a rougher noise.

We point out that different types of noise in the limiting cases as $\beta = 1$ correspond to the space-time white noise (or a finite approximation of it) in Examples 1, 2, and 3 (but not 4), and note that in Figs. 3, 5 and 9 the energy curve levels at the value produced in the limiting case of $\beta = 1$.

5 Influence of noise on global behavior: blow-up probability

In this section, we investigate how a multiplicative perturbation driven by a noise W colored in space and white in time (via our four examples) affects the solutions' global behavior: whether it arrests the blow-up so that the solution exists on much longer time

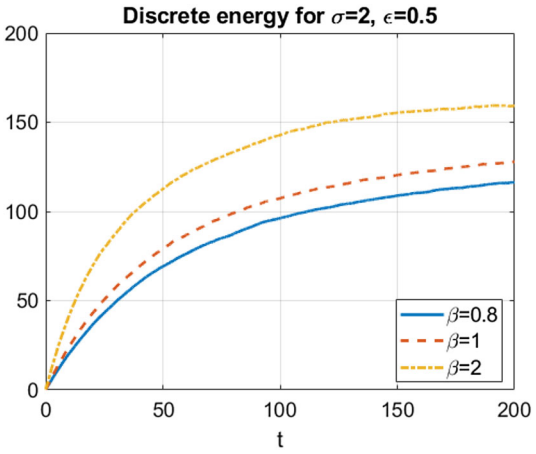

Fig. 12 The growth of energy for different values of β in Example 4 (exponential kernel) on a longer time interval, $0 < t < 200$

intervals, or instead, whether it ceases the global behavior and drives the evolution towards a blow-up.

5.1 Comments about the mesh-refinement

When checking a sufficiently long evolution of solutions considered in the previous two sections, a uniform space mesh was sufficient for the numerical simulations. However, when studying the blowup/scattering thresholds, one needs to be careful, since the uniform mesh may lead to an oscillatory solution at some amplitude, for which the true solution actually would blow up. Such oscillations might be due to the effect of the 4th order derivative residue term from u_{xxxx} when we approximate the discretization of ∂_{xx} by Taylor expansion. (For more details on this we refer the reader to [10,11,17].) In order to avoid this issue, a mesh-refinement can be implemented (for example, as in [11] or [36]) to let the solution evolve in time more accurately in numerical simulations.

As we refine the mesh, we face the recalculation of the covariance matrix. Furthermore, in Examples 3 and 4 (homogeneous noise), a convolution is involved leading to computation of a full covariance matrix and its Cholesky decomposition. This part consumes significant time, and each mesh refinement, for example as we did in [36], would involve an extra recalculation of the covariance matrix, making the computational time prohibitive to obtain any useful results.

Instead, we have a more efficient approach: instead of using a non-uniform mesh refinement, we start by setting *a priori* the central region to be refined enough to reach a height identified as blowup (for example, 5 times that of the initial data: $\|u(t)\|_{L^\infty} = 5\|u_0\|_{L^\infty}$). Outside of the central region, we keep the previously used space mesh. Thus, by refining specific regions in our computational domain from the beginning, the mesh refinement is no longer needed later in the computations. Hence, the Cholesky decomposition for the covariance matrix used in Examples 3 and 4 is done only once in the beginning, saving a large quantity of computational time. We use the computational interval with $L_c = 10$ and set the initial space mesh as follows:

we choose the central region to be $[-1, 1]$ and set $\Delta x = 0.1$ outside of it; inside the central region, that is, for $x \in [-1, 1]$, we set $\Delta x = 0.1/4$. The time mesh we use is $\Delta t = 0.05$. In this Section in our simulations, a solution is identified as *blow-up* if $\|u(t, \cdot)\|_{L^\infty} > 5\|u_0\|_{L^\infty}$, and a solution is identified as *scattering* if the time evolution did not blow up before the time $t = 5$.

5.2 Probability of blow-up

We are now able to investigate the noise influence on the overall behavior of solutions to (1.1). Computationally, the results of this part are the most challenging and time consuming. Computing the covariance matrices and the correlated noise via $\mathcal{A}\chi$ in Examples 3 and 4 takes a significant amount of computational time, as these quantities are full matrices, which need $O(N^2)$ operations. For other operations, such as matrix multiplication when solving linear or non-linear systems in (2.6), (2.7) or (2.8) schemes, we only need $O(N)$ operations as they are sparse systems. In Examples 3 and 4, we use Nvidia RTX 2070 SUPER and Nvidia GTX1080ti GPUs to compute the covariance matrices, since GPUs are much faster in matrix addition and multiplications. Nevertheless, currently it takes approximately 10 hours to generate, for example, the right subplot in Fig. 15 on one of our 18 core Intel i9-7980xe workstations (when using one of the latest versions of Matlab with parallel computing command "parfor"). Furthermore, we also used the HPC[1] to perform computations that we show in Figs. 13, 14, 15 and 16.

For each of the four examples of spatially correlated noise considered, we track the time evolution of solutions with initial data just slightly above the ground state Q. In particular, in the L^2-critical case ($\sigma = 2$) we take initial condition $u_0 = 1.05Q$, and in the L^2-supercritical case (with $\sigma = 3$) we consider $u_0 = 1.01Q$. In the deterministic setting both of these initial conditions lead to a solution blowing up in finite time (and small perturbations of such data also lead to a blow-up in finite time with a similar dynamics). In the stochastic setting any data (even small) can blow-up with a positive probability (see [9]), therefore, to track how the probability of blow-up changes, we have to take the initial conditions very close to Q.

Recall that ϵ is the strength of the noise, which is an important parameter to track for understanding how the noise influences the global behavior. We also investigate how the correlation parameter β influences the blow-up (recall that in the first three examples, $\beta \to 1$ means that the noise W that we use approaches the space-time white noise). We take $\beta \in [0, 1]$ and subdivide this interval into 100 sub intervals (that is, we compute the time evolution of solutions with an increment of 0.01 in β).

We track the probability of blow-up as follows: in the L^2-critical case ($\sigma = 2$) we average over 1000 trials and in the L^2-supercritical case (we work with $\sigma = 3$) we average over 3000 trials in order to obtain a smoother curve of probabilities; indeed, we notice that the probability of blow-up turns out to be higher, and the random blow-up time varies more. As we mentioned, we mark a numerical run as a blow-up solution if the amplitude becomes higher than 5 times of the original amplitude, and we record a run as scattering if the time evolution did not blow-up within the

[1] High Performance Computing (HPC) resources at Florida International University.

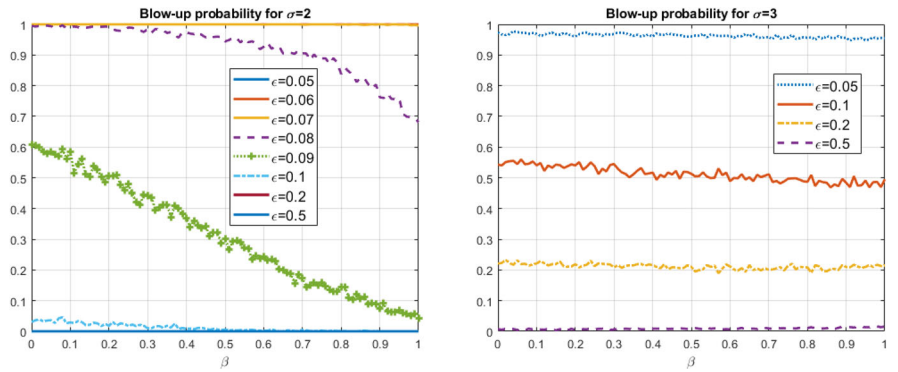

Fig. 13 Blow-up probability for different noise strength ϵ and space correlation β in Example 1 (Gaussian-type decay). Left: L^2-critical ($\sigma = 2$) case. Right: L^2-supercritical ($\sigma = 3$) case

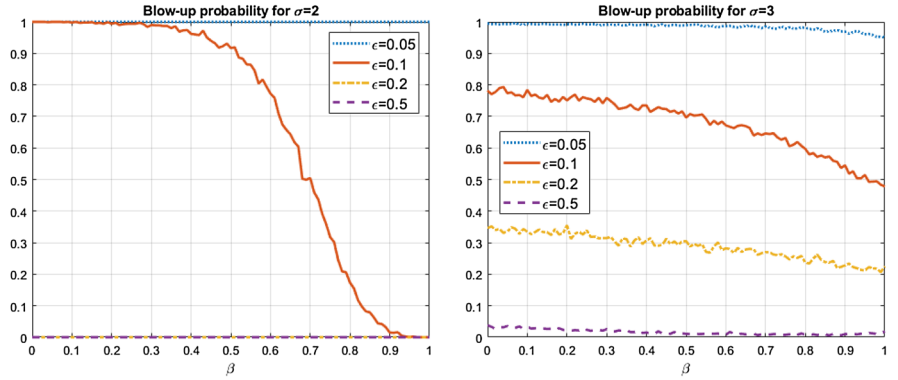

Fig. 14 Blow-up probability for different ϵ and space correlation β in Example 2 (polynomial decay) with $n = 4$. Left: L^2-critical ($\sigma = 2$) case. Right: L^2-supercritical ($\sigma = 3$) case

considered time interval $0 < t \leq 5$. We typically consider values of the noise strength $\epsilon = 0.05, 0.1, 0.2$ and 0.5, though in some instances we had to refine it (for example, in Fig. 13 to pin down the interval which affects the blow-up percentage). The values of the parameters L_c, Δt and Δx are as described in the previous subsection.

In Figs. 13 and 14 we show the probability of blow-up for Example 1 (Gaussian-type decay) and Example 2 (polynomial decay). First, observe that as β increases to 1, the probability of blow-up diminishes; it decreases more significantly in the L^2-critical case than in the L^2-supercritical case. In fact, in the L^2-critical case in Example 1 the noise strength with $\epsilon > 0.09$ seem to eliminate the blow-up completely as $\beta \to 1$, similar dependence is seen in Example 2.

The larger noise strength ϵ tends to drive solutions away from blow-up into a scattering regime (for example, $\epsilon \geq 0.1$ in Fig. 14), while very small values of ϵ let the time evolution keep the blow-up behavior (at least on the considered time interval), for example, see curves for $\epsilon = 0.05$ in both Figs. 13 and 14—they are more easily identified in the right subplots in the L^2-supercritical case, on the very top of the plot.

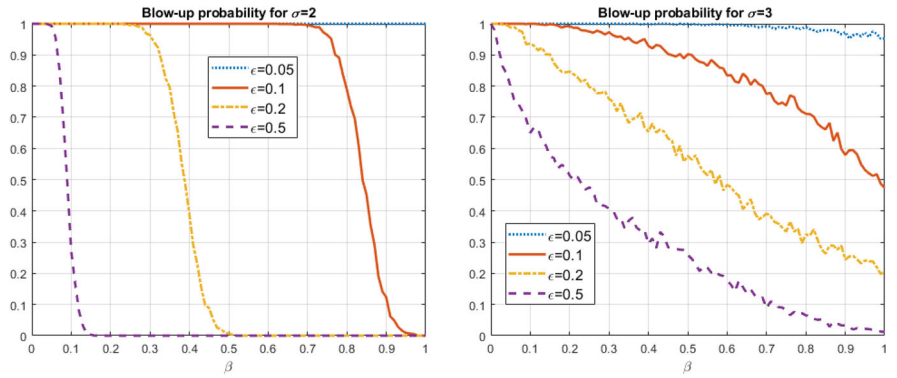

Fig. 15 Blow-up probability for different ϵ and space correlation β in Example 3 (Riesz kernel). Left: L^2-critical ($\sigma = 2$) case. Right: L^2-supercritical ($\sigma = 3$) case

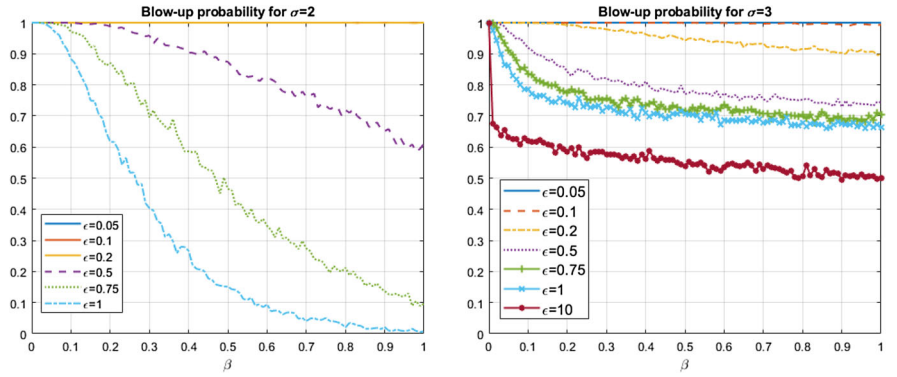

Fig. 16 Blow-up probability for different ϵ and space correlation β in Example 4 (exponential decay). Left: L^2-critical ($\sigma = 2$) case. Right: L^2-supercritical ($\sigma = 3$) case

We next examine the global behavior in Example 3 of a homogeneous noise defined in terms of the Riesz kernel. The probability of blow-up is given in Fig. 15. Note that, as we have a stronger spatial correlation when using this Riesz kernel, the stronger noise tend to arrest blow-up with higher probability and force into the scattering regime. For example, we see no blow-up behavior in solutions in the L^2-critical equation with $\epsilon = 0.5$ starting with $\beta \geq 0.15$; see left plot in Fig. 15.

Finally, we show the probability of blow-up in Example 4 (exponential kernel, $e^{-\beta|x|}$) in Fig. 16. On the left it is the L^2-critical case and on the right it is the L^2-supercritical case ($\sigma = 3$). As with the Riesz kernel, we observe that a larger noise strength (such as $\epsilon = 0.5$) tends to arrest blow-up in an increasing number of cases as β increases (note that β can go beyond 1 in this example), and it can almost eliminate blow-up, at least in the L^2-critical case (see $\epsilon = 1$ curve on the left subplot of Fig. 16). Note that in the L^2-supercritical case in the Example 4, while the probability of scattering slightly increases with growing β and with increasing ϵ, the blow-up probability curve is not affected as dramatically as in the L^2-critical case. We were able to track the values of ϵ higher than 1: an example of $\epsilon = 10$ is shown on the

right subplot of Fig. 16. (In this case we did $N_t = 2000$ trials; a visible initial jump is because for computational purposes when $\beta = 0$, we take $\epsilon = 0$.) Thus, the blow-up probability curves in Fig. 16 (also in Figs. 13 and 14) are different from the L^2-critical case, which corroborates the result in [9] that in the L^2-supercritical case *any* sufficiently smooth and sufficiently localized data blows-up in finite time with positive probability. We also observe that the stronger the nonlinearity is ($\sigma = 3$ vs. $\sigma = 2$) the more resistance to scattering time evolution has.

Summarizing, in all our examples of spatially-correlated noise, we observe that a larger noise strength ϵ and more concentrated space-correlation (higher value of β) help prevent or delay the blow-up, hence, forcing solutions to exist for longer time. We emphasize that the above simulations were done with the initial data that leads to blow-up in finite time in the deterministic case ($\epsilon = 0$).

Finally, we want to make a remark about a reverse phenomenon, i.e., when initial data, which in the deterministic case generate solutions existing globally in time (moreover, scattering), can in the stochastic case produce a time evolution, which blows up in finite, though random, time with positive probability. For example, in Example 3 (Riesz kernel) when taking $u_0 = 0.99Q$, $\epsilon = 0.2$, and considering the L^2-supercritical case $\sigma = 3$, we observed 1 or 2 blow-up trajectories out of 1000 runs for the values of $\beta = 0.25, 0.5$, or 0.75. While the probability is very low, it is positive; this is consistent with results proved in [9, Thm 5.1]. We ran a similar experiment in the L^2-critical case and did not observe any blow-up trajectories in 2000 runs for a variety of values of β; this is consistent with [35, Thm 2.7]. We conclude this section with mentioning that a similar positive probability of blow-up in finite time we observed in the case of space-time white noise in [36, end of Sect. 5].

6 Effect of the noise on blow-up dynamics

In this section we show how the finite-time blow-up dynamics (rates and profiles) might be affected by the spatially-correlated driving noise. To track the blow-up behavior we use the algorithm we introduced in [36, Sect. 4]. Note that the blow-up time is a random time $T = T(\omega)$. To avoid reaching the blow-up time $T(\omega)$, we use the non-uniform mesh in time, i.e., $\Delta t_m = \dfrac{\Delta t_0}{\|u(t_m, x)\|_{L^\infty}^{2\sigma}}$, where $t_0 = 0$ and $t_m = \sum_{l=0}^{m-1} \Delta t_l$ is the mth time step.

We also use the spatial mesh-refinement. Unlike the previous section, where we can *a priori* preset the non-uniform mesh, here, we need to keep refining the mesh as time evolves. Therefore, the interpolation for the solution on the new grid points is needed. We apply our new mesh-refinement strategy with the mass-conservative interpolation,[2] introduced in [36, Sect. 4] for the value of $u(t_m, \tilde{x}_j)$ at the new grid points $\tilde{x}_j$ at time t_m. This, however, results in the covariance matrices being recomputed and updated at each mesh refinement, slowing down the computations. We first check the accuracy of our approach by computing the difference of the mass at different times (for both discrete as in (1.2) and its approximation via the composite trapezoid rule, see (4.10)

[2] The new part in this interpolation is that the mass is preserved before and after the refinement of a spatial interval, see [36, (4.8) and Fig. 14].

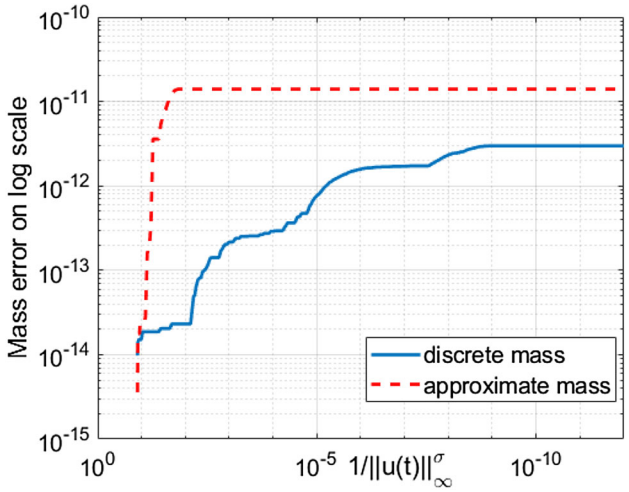

Fig. 17 Error in mass computation of a blow-up trajectory with $u_0 = 3e^{-x^2}$ in Example 3 (Riesz kernel) with $\beta = 0.5$ in the L^2-supercritical case ($\sigma = 3$)

and (4.11) in [36] for the definition) in the case of blow-up solutions; see Fig. 17. We observe that our schemes preserve mass very accurately (at least 10^{-11} or more precisely) during the blow-up evolution.

A word of caution should be made about the refinements. It was already noted in [10] that a refinement can affect the outcome of simulations of the global behavior quite severely (e.g., coarser mesh grids can allow the singularity to form, and the finer mesh grids can prevent or delay the blow-up), this also depends on the type of refinement used (in [10] it was a classical linear interpolation, which does not preserve mass). In our implementation of mesh-refinement, we use a mass-conservative approach, which can be viewed as a next step in investigating blow-up in the stochastic setting. We show that it is sufficiently accurate and robust method to obtain information about the blow-up dynamics. It will be important to investigate further the formation of blow-up and the blow-up dynamics, and in particular, influence of the refinement onto the blow-up; in this work we initiate the study of blow-up dynamics for the white in time colored in space multiplicative stochastic perturbations, with some examples approaching the space-time white noise.

In what follows we track blow-up dynamics in both the L^2-critical and L^2-supercritical cases. In these simulations we average over 100 runs. To make sure that the time evolution leads to a blow up behavior, we choose the initial condition $u_0 = A\, e^{-x^2}$ with $A \geq 3$ (in both critical and supercritical cases). We set $\Delta t_0 = 0.002$ and the initial uniform grid mesh size $\Delta x = 0.05$ on $x \in [-L_c, L_c]$ with $L_c = 5$ (as the blow-up is a local phenomenon, a larger value of L_c is unnecessary). We stop our simulations when $\|u\|^{\sigma}_{L^\infty}$ reaches 10^{10}, or equivalently, $L(t) \sim 10^{-10}$. For a review on blow-up dynamics, we refer the reader to [36, Introduction], [45] (for the L^2-critical case), [46] (for the L^2-supercritical case), or see monographs [17,42] and references therein.

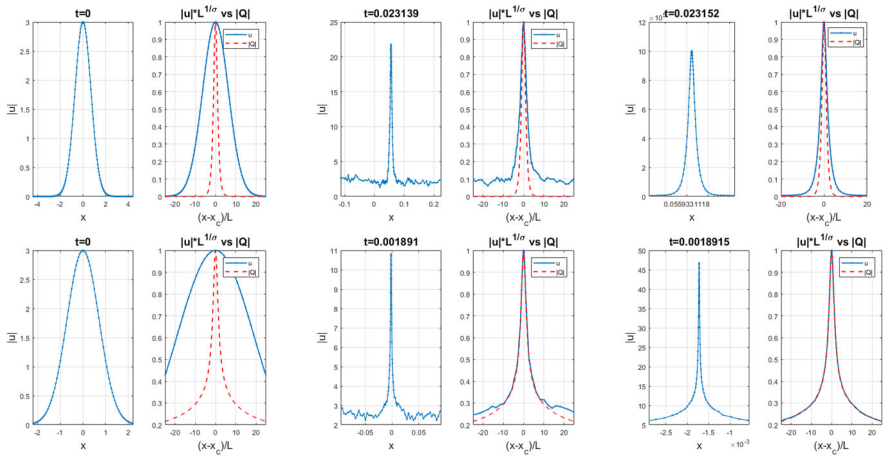

Fig. 18 Formation of blow-up in Example 2 (polynomial decay) with $n = 4$, $\beta = 0.5$ and $\epsilon = 0.1$: snapshots of time evolution for $u_0 = 3\,e^{-x^2}$ (given in pairs of actual and rescaled solution) at different times. Each pair of graphs shows in solid blue the actual solution $|u|$ and its rescaled version $L^{1/\sigma}|u|$, comparing it to the normalized ground state Q in dashed red. Top row: L^2-critical ($\sigma = 2$) case (blow-up smooths out and converges slowly to the ground state Q). Bottom row: L^2-supercritical ($\sigma = 3$) case (blow-up profile becomes smooth and converges faster to the profile $Q_{1,0}$)

We start with tracking the blow-up profiles. Figure 18 shows snapshots of blow-up solutions at different times for Example 2 (polynomial decay). The top row shows the case of the L^2-critical blow-up; one can see that the solution smooths and converges slowly to the ground state Q. (The reason for the slow convergence is the same as in the deterministic case: the shown regime is still far from the high focusing level needed to observe the convergence.) The bottom row shows the blow-up in the L^2-supercritical case ($\sigma = 3$). Observe that in this case the solution smooths out and converges to the (rescaled) profile solution $Q_{1,0}$ fast; see the right bottom plot in Fig. 18. We also show the convergence of the solution in a homogeneous noise Example 4 (exponential decay) in Fig. 19, observing a similar convergence behavior. The other two examples are in "Appendix B" in Figs. 26 and 29.

To determine blow-up rates, we check the time dependence of $L(t)$. We take $L(t) = \|\nabla u(t)\|_{L^2}^{-(1-s)}$ (note that in the deterministic case it is typical to take $L(t) = \|u(t)\|_{L^\infty}^{-\sigma}$); however, here, we define $L(t)$ via the L^2-norm of the gradient, since it gives a more stable computation for the parameter a below; both definitions are equivalent for $s < 1$, see [17]). In the left subplots of Fig. 20 we show the logarithmic dependence of $L(t)$ on $T - t$. Note that in both the critical and supercritical cases, the slope is 0.5, that is, solutions blow up with a rate $L(t) \sim \sqrt{T-t}$, possibly with some correction terms.

To investigate the correction terms we study the convergence of the parameter $a(t)$ as $t \to T(\omega)$, or equivalently, behavior of $a(\tau)$ as $\tau \to \infty$ in the rescaled time $\tau = \int_0^t \frac{1}{L^2(s)} ds$, or $\frac{d\tau}{dt} = \frac{1}{L^2(t)}$ (then, $t \to T$ is equivalent to $\tau \to \infty$). As discussed

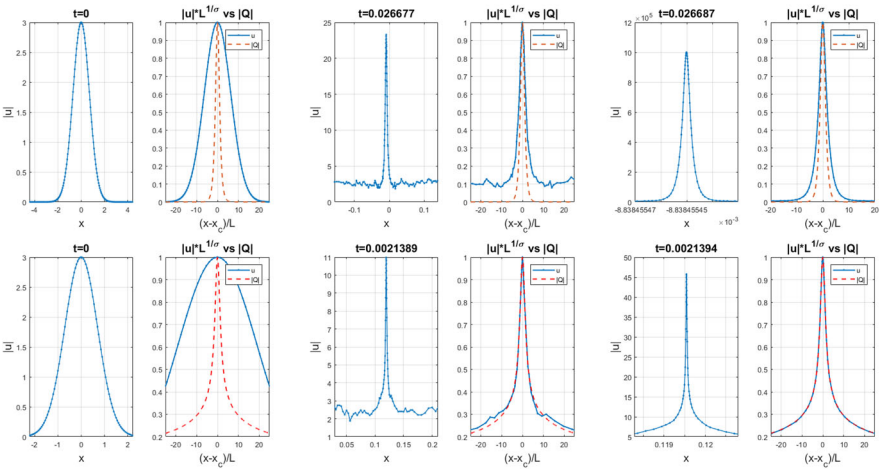

Fig. 19 Formation of blow-up in Example 4 (exponential kernel) with $\beta = 0.5$ and $\epsilon = 0.1$, for other details, see Fig. 18

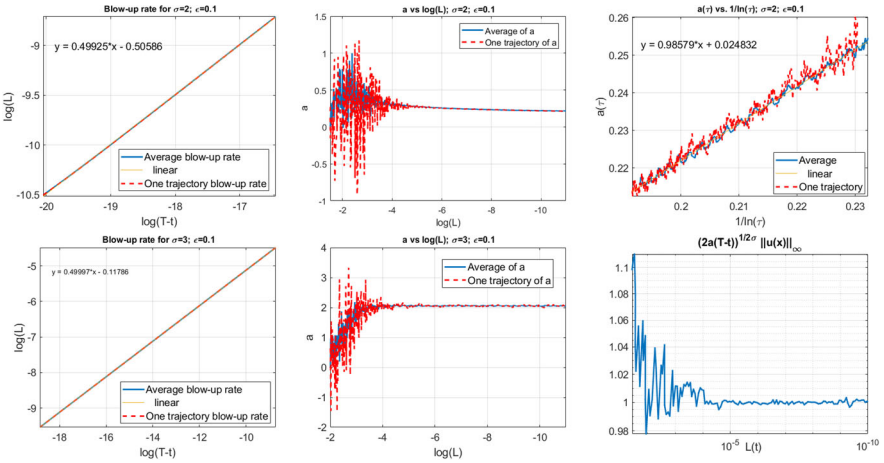

Fig. 20 Blow-up rate tracking in Example 2 (polynomial decay) with $n = 4$, $\beta = 0.5$ and $\epsilon = 0.1$. Top row: L^2-critical ($\sigma = 2$) case. Bottom row: L^2-supercritical case. Left: logarithmic dependence of $\log L(t)$ vs. $\log(T-t)$ (note in both cases the slope is 0.50). Middle: $a(\tau_m)$ vs. $\log L(\tau_m)$ (an extremely slow decay to zero in the top plot and rather fast leveling at a constant level in the bottom plot). Right top: dependence $a(\tau)$ vs. $1/\ln(\tau)$ to confirm the logarithmic correction. Right bottom: fast convergence to a constant 1 of the quantity $\|u\|_{L^\infty}\,(2a(T-t))^{\frac{1}{2\sigma}}$

in the introduction, we set $a(t) = -L_t\,L$. A direct calculation (see also [36,42]) yields

$$a(t) = -\frac{2}{\alpha}\,\frac{1}{(\|\nabla u(t)\|_{L^2}^2)^{\frac{2}{\alpha}+1}}\int |u(t)|^{2\sigma}\,\mathrm{Im}(u_{xx}(t)\,\bar{u}(t))\,dx, \qquad \alpha = 1+\frac{2}{\sigma}.$$

In the discrete version, we take $\Delta\tau = \Delta t_0$ with $\tau_m = m \cdot \Delta t_0$ as a rescaled time. Then at the mth step we obtain values $L(\tau_m)$, $u(\tau_m)$, and $a(\tau_m)$. We track the behavior of $a(\tau)$ vs. $\log L(\tau)$, which is shown in the middle subplots of Figs. 20 and 21 (see also Figs. 28 and 29): the red dashed curve shows the behavior for one trajectory of a and the blue solid line shows an averaged over 100 runs behavior. Observe that in the L^2-supercritical case (bottom middle plot), $a(\tau)$ converges to a constant after 4 orders of magnitude of L, while in the L^2-critical case (top middle plot) $a(\tau)$ decays very slowly (to zero). This is similar to the deterministic case. We also track the dependence of $a(\tau)$ on $1/\ln\tau$ (as in the deterministic case) to show that the correction to the rate in the L^2-critical case is slower than any polynomial power correction. This gives a confirmation that the correction is of a logarithmic order. Our conjecture is that in the SNLS equation, the correction in the L^2-critical case is a double log correction (1.11), similar to the deterministic case, though it is a highly nontrivial task to show it (as in the deterministic case) and requires further studies. Nevertheless, the above findings give partial confirmation to the blow-up dynamics stated in Conjecture 1.

To further justify Conjecture 1 about the double log correction in the rate, we give arguments similar to the deterministic case (see [45,47] or [42, Chapter 8.2]). As numerically observed in Fig. 20, $a(\tau)$ decays as $\frac{1}{\ln(\tau)}$. We write $L(t) = (T-t)^{\frac{1}{2}} q(t)$ with $q(t)$ being a slow varying term such that its derivative $q'(t)$ is negligible. Integrating $\frac{d\tau}{dt} = \frac{1}{L^2(t)}$, we will get the leading order of τ to be

$$\tau = \int \frac{1}{L^2(t)} dt = -\ln(T-t) q^{-2}(t) + \frac{2}{T-t} \frac{q'(t)}{q^3(t)} \approx \ln\left(\frac{1}{T-t}\right) \frac{1}{q^2(t)}, \quad (6.1)$$

provided $q(t)$ varies slower than $\ln(\frac{1}{T-t})$. Then it is reasonable to assume that

$$a \sim \frac{1}{\ln(\ln(\frac{1}{T-t}))},$$

(for example, as we did with functional fitting in [45]). On the other hand, note that

$$\begin{aligned} a(t) &= -L(t)L'(t) \\ &= -(T-t)^{\frac{1}{2}} q(t) \cdot \left(-\frac{1}{2}(T-t)^{-\frac{1}{2}} q(t) - (T-t)^{\frac{1}{2} q'(t)} \right) \approx \frac{1}{2} q^2(t), \end{aligned}$$

which implies

$$q(t) \sim \left(\frac{1}{\ln\ln(\frac{1}{T-t})} \right)^{\frac{1}{2}}.$$

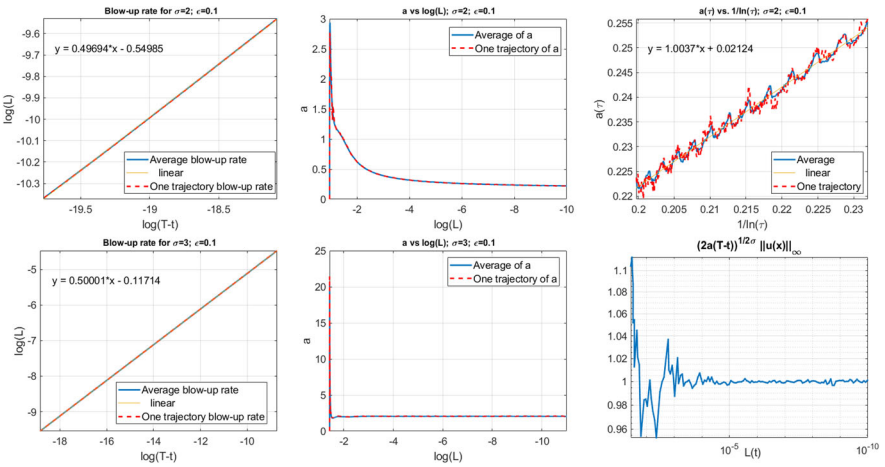

Fig. 21 Blow-up rate tracking in Example 4 (exponential kernel) with $\beta = 0.5$ and $\epsilon = 0.1$. Top row: L^2-critical ($\sigma = 2$) case. Bottom row: L^2-supercritical case. Left: logarithmic dependence of $\log L(t)$ vs. $\log(T - t)$ (note in both cases the slope is 0.50). Middle: $a(\tau_m)$ vs. $\log L(\tau_m)$ (decay to zero in the top plot and an almost immediate leveling at a constant level in the bottom plot). Right top: dependence $a(\tau)$ vs. $1/\ln(\tau)$ to confirm the logarithmic correction. Right bottom: fast convergence to a constant 1 of the quantity $\|u\|_{L^\infty}(2a(T-t))^{\frac{1}{2\sigma}}$

Observe that this also matches our assumption that $q(t)$ varies slower than $\ln \frac{1}{T-t}$. Putting the estimates together, we obtain

$$L(t) \sim \left(\frac{T-t}{\ln \ln(\frac{1}{T-t})} \right)^{\frac{1}{2}}, \tag{6.2}$$

which explains the log-log blow-up rate in the L^2-critical case (Conjecture 1).

In the L^2-supercritical case, we note that $a(t)$ converges to a constant a. Using again the fact that $a(t) = -L(t)L'(t) = -\frac{1}{2}(L^2(t))'$, we solve the ODE

$$a = -\frac{1}{2}(L^2(t))', \qquad L(T) = 0,$$

where the boundary condition $L(T) = 0$ comes from the fact that $\|u(t)\|_{L^\infty} = \infty$ at $t = T$. Thus, we obtain

$$L(t) = \sqrt{2a\,(T-t)},$$

explaining the rate in Conjecture 2. Observe that the convergence of $a(t)$ to the constant a is very fast in the supercritical case, which is confirmed in the bottom right subplot of Fig. 29, justifying the above explanation for the time dependence of $L(t)$, and hence, the rate in Conjecture 2.

In [36] we observed that the noise affects the location of the blow-up center, and shifts it away from the origin (or from the original peak location), making it a random

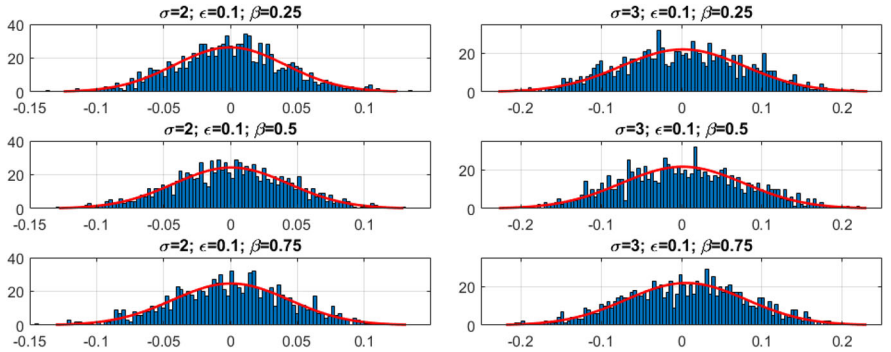

Fig. 22 Location distribution of the blow-up center x_c in Example 1 for different β from 1000 runs. Here, $u_0 = 3e^{-x^2}$ and $\epsilon = 0.1$. Left: $\sigma = 2$. Right: $\sigma = 3$

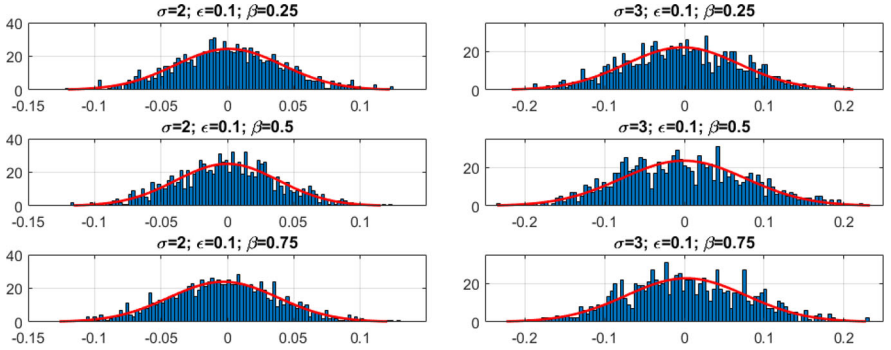

Fig. 23 Location distribution of the blow-up center x_c in Example 2 (polynomial decay) with $n = 2$ for different β from 1000 runs. Here, $u_0 = 3e^{-x^2}$ and $\epsilon = 0.1$. Left: $\sigma = 2$. Right: $\sigma = 3$

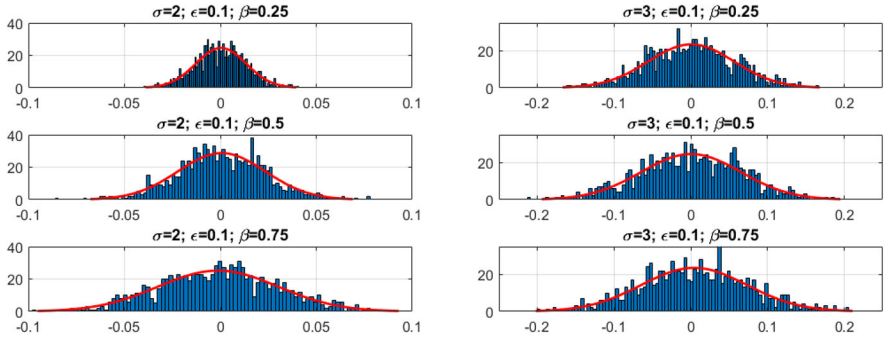

Fig. 24 Location distribution of the blow-up center x_c in Example 3 (Riesz kernel) for different β from 1000 runs. Here, $u_0 = 3e^{-x^2}$ and $\epsilon = 0.1$. Left: $\sigma = 2$. Right: $\sigma = 3$

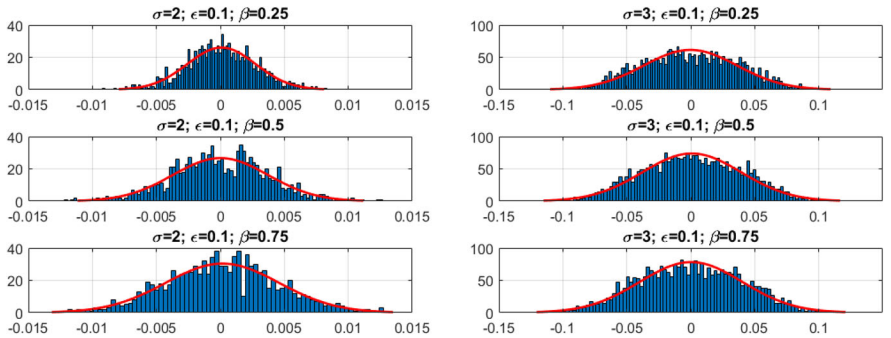

Fig. 25 Location distribution of the blow-up center x_c in Example 4 (exponential kernel) for different β. Here, $u_0 = 3e^{-x^2}$ and $\epsilon = 0.1$. Left: $\sigma = 2$ with 1000 runs. Right: $\sigma = 3$ with 3000 runs (compare this much smoother convergence to a normal distribution with Fig. 24 with 1000 runs)

variable distributed normally. In this work we also check the location of blow-up centers for different runs; see Figs. 22, 23, 24 and 25 for the distribution curves (we did 1000 runs, except for the right graph in Fig. 25 with $N_t = 3000$ runs) and Tables 1 and 3 for the mean and variance in each of our four examples in the L^2-critical and supercritical cases ($\sigma = 3$) with different correlation parameters β. Our findings confirm the normal distribution of the curves (conditionally to the existence of blow-up), and that the shifting is more prominent in the L^2-supercritical case (larger variance); the variance also grows with the correlation parameter β in the supercritical case (see Table 1, 2, 3 and 4). The mean of the distribution varies but remains quite small; we think that with a larger number of trials it would converge to zero.

We conclude that the spatially-correlated noise has little effect on the blow-up dynamics, similar to our findings in [36] for the approximation of the space-time white noise. In particular, the driving noise considered in this paper has almost no effect on the blow-up profiles and rates, but shifts the location of the blow-up center.

7 Conclusion

In this paper we investigate how solutions behave in the 1D focusing SNLS subject to a multiplicative stochastic perturbation driven by a space-correlated Wiener process. We consider four different examples of space-correlation, where the noise is either driven by $\mathcal{Q}$-Brownian motions, thus, with a trace-class (diagonal) covariance operator, or by a homogeneous Wiener process, where the covariance matrix is no longer diagonal and has longer range effects. Due to the Stratonovich integral, the mass is conserved in this stochastic setting; however, the energy (or Hamiltonian) changes in time. We observe that in our examples the energy grows first and then levels off to a horizontal asymptote whose value is close to a corresponding one in the case of the space-time white noise (to be precise, the approximation of it). We then investigate the effect of the spatially-correlated noise onto the probability of blow-up. We note that a larger strength of the stochastic perturbation and a greater concentration close to the origin

for spatially correlated driving noises tend to decrease the probability of blow-up in both L^2-critical and supercritical cases, though bearing more influence in the critical case. In the supercritical case we also observe that the spatially-correlated noise can drive the evolution towards the blow-up for the initial data that in the deterministic setting would generate solutions existing globally and scattering (to linear solutions). This is in agreement with results proved in [9] for a regular driving noise, and with our previous numerical findings in [36] for the SNLS equation driven by an approximation of the space-time white noise. Finally, we study the blow-up dynamics, and confirm that the spatially-correlated noise as we consider in this work has almost no influence on profiles or rates of the blow-up, and only affects the location of the blow-up center. This is similar to our findings for the space-time white noise in [36]. Once the evolution is driven into the blow-up regime, the dynamics except for the blow-up center location is the same as in the deterministic case.

Acknowledgements Part of this work was done when the first author visited Florida International University. She would like to thank FIU for the hospitality and the financial support. A.M.'s research has been conducted within the FP2M federation (CNRS FR 2036). S.R. was partially supported by the NSF Grant DMS-1815873/1927258 as well as part of the K.Y.'s research and travel support to work on this Project came from the above Grant. A.D.R. was supported by REU under DMS-1927258 (PI: Roudenko).

Appendix A

In this appendix we show the distribution of the locations of blow-up center x_c as its being influenced by the noise. We provide Figs. 22, 23, 24 and 25 for each of our four examples when we run $N_t = 1000$ trials in most of them except for the right part in Fig. 25, where we did $N_t = 3000$ trials (note how much more accurate the convergence to the normal distribution is, however, this takes significantly larger computational efforts.) In Tables 1, 2, 3 and 4 we record the mean μ_{x_c} and variance $\sigma^2_{x_c}$ of the normal distribution that we obtain for the location random variable x_c. Observe that the variance noticeably increases in Examples 3 and 4 in the L^2-critical case as β increases (similar increase is happening in these Examples in the L^2-supercritcal case, see Tables 3 and 4).

Table 1 Mean μ_{x_c} and variance $\sigma^2_{x_c}$ of the location of blow-up center random variable x_c. Example 1 (Gaussian decay) shown in Fig. 22.

σ	β	μ_{x_c}	$\sigma^2_{x_c}$
2	0.25	−2.4e−4	0.0013
2	0.5	−5.7e−4	0.0014
2	0.75	−4.1e−4	0.0014
3	0.25	0.0017	0.0024
3	0.5	0.0014	0.0024
3	0.75	0.0059	0.0024

Table 2 Table 2 Mean μ_{x_c} and variance $\sigma^2_{x_c}$ of the location of blow-up center random variable x_c. Example 2 (polynomial decay, $n = 2$) shown in Fig. 23

σ	β	μ_{x_c}	$\sigma^2_{x_c}$
2	0.25	0.0011	0.0013
2	0.5	−1.3e−4	0.0012
2	0.75	−0.003	0.0013
3	0.25	−0.0023	0.0023
3	0.5	−9e−4	0.0025
3	0.75	0.0023	0.0024

Table 3 Mean μ_{x_c} and variance $\sigma^2_{x_c}$ of the location of blow-up center random variable x_c. Example 3 (Riesz kernel) shown in Fig. 24.

σ	β	μ_{x_c}	$\sigma^2_{x_c}$
2	0.25	3.3e−4	4.1e−4
2	0.5	6.6e−4	7.2e−4
2	0.75	−0.0012	9.9e−4
3	0.25	5.3e−4	0.0018
3	0.5	3.5e−4	0.0020
3	0.75	0.0044	0.0022 s

Table 4 Mean μ_{x_c} and variance $\sigma^2_{x_c}$ of the location of blow-up center random variable x_c Example 4 (exponential kernel) shown in Fig. 25

σ	β	μ_{x_c}	$\sigma^2_{x_c}$
2	0.25	8.8e−5	8.5e−5
2	0.5	5.4e−6	1.2e−4
2	0.75	1.6e−4	1.4e−4
3	0.25	−3.3e−4	6.7e−4
3	0.5	7.9e−4	7.0e−4
3	0.75	2.1e−4	7.4e−4

Appendix B

Here we show Figs. 26, 27, 28 and 29 of blow-up dynamics (convergence of profiles and rates) in Examples 1 and 3.

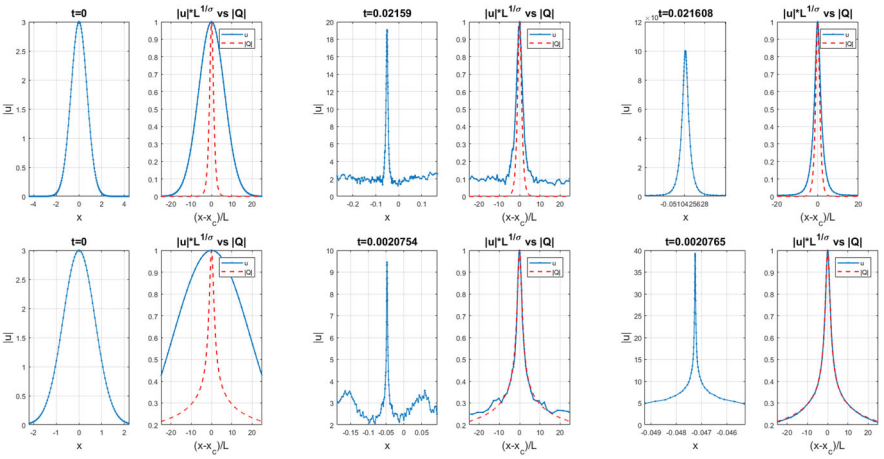

Fig. 26 Formation of blow-up in Example 1 (exponential decay) with $\beta = 0.5$ and $\epsilon = 0.1$: snapshots of time evolution for $u_0 = 3\,e^{-x^2}$ (given in pairs of actual and rescaled solution) at different times. Each pair of graphs shows in solid blue the actual solution $|u|$ and its rescaled version $L^{1/\sigma}|u|$, comparing it to the normalized ground state Q in dashed red. Top row: L^2-critical ($\sigma = 2$) case (blow-up smooths out and converges slowly to the ground state Q). Bottom row: L^2-supercritical ($\sigma = 3$) case (blow-up profile becomes smooth and converges faster to the profile $Q_{1,0}$)

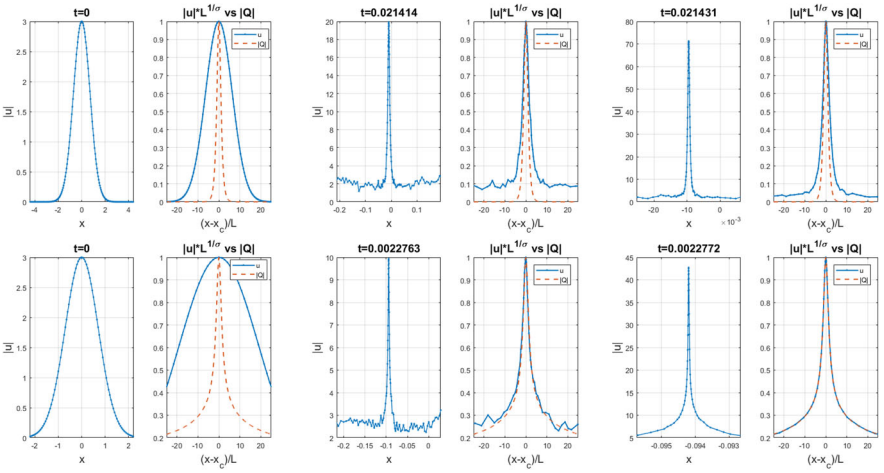

Fig. 27 Formation of blow-up in Example 3 (Riesz kernel) with $\beta = 0.5$ and $\epsilon = 0.1$: snapshots of time evolution for $u_0 = 3\,e^{-x^2}$. For other details, see Fig. 26

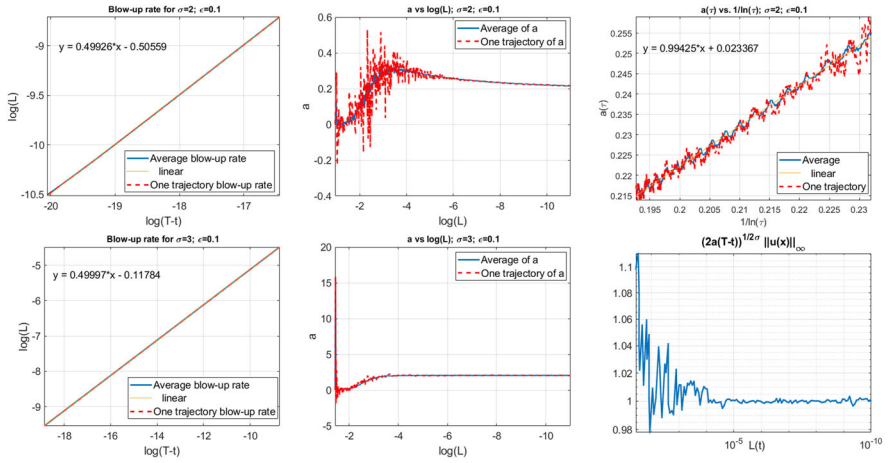

Fig. 28 Blow-up rate tracking in Example 1 (exponential decay) with $\beta = 0.5$ and $\epsilon = 0.1$. Top row: L^2-critical ($\sigma = 2$) case. Bottom row: L^2-supercritical case. Left: logarithmic dependence of $\log L(t)$ vs. $\log(T - t)$ (note in both cases the slope is 0.50). Middle: $a(\tau_m)$ vs. $\log L(\tau_m)$ (an extremely slow decay to zero in the top plot and rather fast leveling at a constant level in the bottom plot). Right top: dependence $a(\tau)$ vs. $1/\ln(\tau)$ to confirm the logarithmic correction. Right bottom: fast convergence to a constant of the quantity $\|u\|_{L^\infty}(2a(T-t))^{\frac{1}{2\sigma}}$

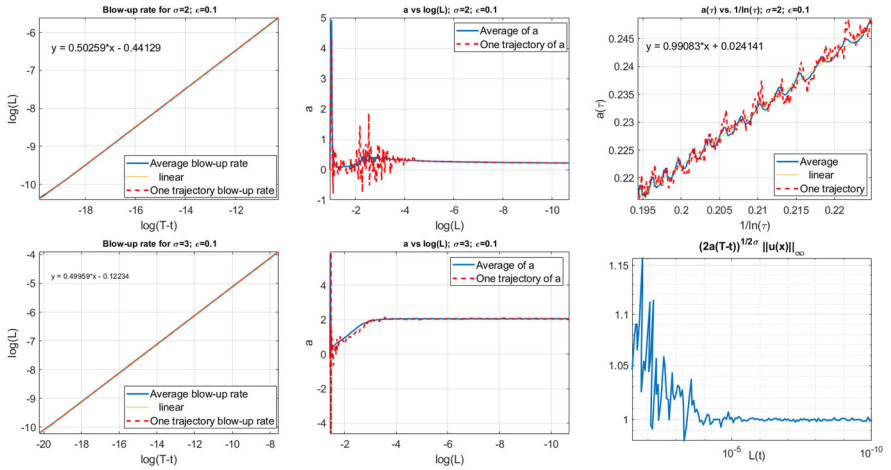

Fig. 29 Blow-up rate tracking in Example 3 (Riesz kernel) with $\beta = 0.5$ and $\epsilon = 0.1$. For details, see Fig. 28

References

1. Bang, O., Christiansen, P., If, F., Rasmussen, K., Gaididei, Y.: Temperature effects in a nonlinear model of monolayer Scheibe aggregates. Phys. Rev. E **49**, 4627–4636 (1994)
2. Budd, C.J., Chen, S., Russell, R.D.: New self-similar solutions of the nonlinear Schrödinger equation with moving mesh computations. J. Comput. Phys. **152**(2), 756–789 (1999)
3. Cazenave, T.: Semilinear Schrödinger Equations, Volume of Courant Lecture Notes in Mathematics, vol. 10. New York University, Courant Institute of Mathematical Sciences, New York (2003)
4. Cazenave, T., Weissler, F.B.: The Cauchy problem for the critical nonlinear Schrödinger equation in H^s. Nonlinear Anal. **14**(10), 807–836 (1990)
5. Da Prato, G., Zabczyk, J.: Stochastic Equations in Infinite Dimensions, Volume 152 of Encyclopedia of Mathematics and Its Applications, 2nd edn. Cambridge University Press, Cambridge (2014)
6. Dalang, R.: Extending the martingale measure stochastic integral with applications to spatially homogeneous S.P.D.E.'s. Electron. J. Probab. **4**, 29 (1999)
7. de Bouard, A., Debussche, A.: On the effect of a noise on the solutions of the focusing supercritical nonlinear Schrödinger equation. Probab. Theory Relat. Fields **123**(1), 76–96 (2002)
8. de Bouard, A., Debussche, A.: The stochastic nonlinear Schrödinger equation in H^1. Stoch. Anal. Appl. **21**(1), 97–126 (2003)
9. de Bouard, A., Debussche, A.: Blow-up for the stochastic nonlinear Schrödinger equation with multiplicative noise. Ann. Probab. **33**(3), 1078–1110 (2005)
10. Debussche, A., Di Menza, L.: Numerical resolution of stochastic focusing NLS equations. Appl. Math. Lett. **15**(6), 661–669 (2002)
11. Debussche, A., Di Menza, L.: Numerical simulation of focusing stochastic nonlinear Schrödinger equations. Phys. D **162**(3–4), 131–154 (2002)
12. Dodson, B.: Global well-posedness and scattering for the mass critical nonlinear Schrödinger equation with mass below the mass of the ground state. Adv. Math. **285**, 1589–1618 (2015)
13. Duyckaerts, T., Holmer, J., Roudenko, S.: Scattering for the non-radial 3D cubic nonlinear Schrödinger equation. Math. Res. Lett. **15**(6), 1233–1250 (2008)
14. Duyckaerts, T., Roudenko, S.: Threshold solutions for the focusing 3d cubic Schrödinger equation. Rev. Mat. Iberoam. **26**(1), 1–56 (2010)
15. Duyckaerts, T., Roudenko, S.: Going beyond the threshold: scattering and blow-up in the focusing NLS equation. Comm. Math. Phys. **334**(3), 1573–1615 (2015)
16. Fang, D., Xie, J., Cazenave, T.: Scattering for the focusing energy-subcritical nonlinear Schrödinger equation. Sci. China Math. **54**(10), 2037–2062 (2011)
17. Fibich, G.: The nonlinear Schrödinger equation: singular solutions and optical collapse. In: Applied Mathematical Sciences, vol. 192. Springer, Berlin (2015)
18. Fibich, G., Merle, F., Raphaël, P.: Proof of a spectral property related to the singularity formation for the L^2 critical nonlinear Schrödinger equation. Phys. D **220**(1), 1–13 (2006)
19. Ginibre, J., Velo, G.: On a Class of Nonlinear Schrödinger Equations. I. The Cauchy Problem, General Case. J. Funct. Anal. **32**(1), 1–32 (1979)
20. Ginibre, J., Velo, G.: The global Cauchy problem for the nonlinear Schrödinger equation revisited. Ann. Inst. H. Poincaré Anal. Non Linéaire **2**(4), 309–327 (1985)
21. Guevara, C.D.: Global behavior of finite energy solutions to the d-dimensional focusing nonlinear Schrödinger equation. Appl. Math. Res. Express AMRX **2**, 177–243 (2014)
22. Holmer, J., Platte, R., Roudenko, S.: Blow-up criteria for the 3D cubic nonlinear Schrödinger equation. Nonlinearity **23**(4), 977–1030 (2010)
23. Holmer, J., Roudenko, S.: On blow-up solutions to the 3D cubic nonlinear Schrödinger equation. Appl. Math. Res. Express AMRX **1**, 31 (2007)
24. Holmer, J., Roudenko, S.: Divergence of infinite-variance nonradial solutions to the 3D NLS equation. Commun. Part. Differ. Equ. **35**(5), 878–905 (2010)
25. Kato, T.: On nonlinear Schrödinger equations. Ann. Inst. H. Poincaré Phys. Théor. **46**(1), 113–129 (1987)
26. Kopell, N., Landman, M.: Spatial structure of the focusing singularity of the nonlinear Schrödinger equation: a geometrical analysis. SIAM J. Appl. Math. **55**(5), 1297–1323 (1995)
27. LeMesurier, B., Papanicolaou, G., Sulem, C., Sulem, P.-L.: The focusing singularity of the nonlinear Schrödinger equation. In: Directions in Partial Differential Equations (Madison, WI, 1985), Volume 54

of Publication of the Mathematics Research Center, the University of Wisconsin, pp. 159–201. Academic Press, Boston, MA (1987)
28. Lifshits, M.: Lectures on Gaussian Processes. Springer, Berlin (2012)
29. Merle, F.: Determination of blow-up solutions with minimal mass for nonlinear Schrödinger equations with critical power. Duke Math. J. **69**(2), 427–454 (1993)
30. Merle, F., Raphael, P.: Sharp upper bound on the blow-up rate for the critical nonlinear Schrödinger equation. Geom. Funct. Anal. **13**(3), 591–642 (2003)
31. Merle, F., Raphael, P.: The blow-up dynamic and upper bound on the blow-up rate for critical nonlinear Schrödinger equation. Ann. Math. (2) **161**(1), 157–222 (2005)
32. Merle, F., Raphael, P.: Profiles and quantization of the blow up mass for critical nonlinear Schrödinger equation. Commun. Math. Phys. **253**(3), 675–704 (2005)
33. Merle, F., Raphaël, P.: Blow up of the critical norm for some radial L^2 super critical nonlinear Schrödinger equations. Am. J. Math. **130**(4), 945–978 (2008)
34. Merle, F., Raphaël, P., Szeftel, J.: Stable self-similar blow-up dynamics for slightly L^2 super-critical NLS equations. Geom. Funct. Anal. **20**(4), 1028–1071 (2010)
35. Millet, A., Roudenko, S.: Well-posedness for the focusing stochastic critical and supercritical nonlinear Schrödinger equaion. Preprint (2020)
36. Millet, A., Roudenko, S., Yang, K.: Numerical study of solutions behavior to the 1d stochastic L^2-critical and supercritical nonlinear Schrödinger equation (2020). arXiv:2005.14266
37. Perelman, G.: Evolution of adiabatically perturbed resonant states. Asymptot. Anal. **22**(3–4), 177–203 (2000)
38. Perelman, G.: On the formation of singularities in solutions of the critical nonlinear Schrödinger equation. Ann. Henri Poincaré **2**(4), 605–673 (2001)
39. Rasmussen, K., Gaididei, Y., Bang, O., Christiansen, P.: The influence of noise on critical collapse in the nonlinear Schrödinger equation. Phys. Rev. A **204**, 121–127 (1995)
40. Rottschäfer, V., Kaper, T.J.: Blowup in the nonlinear Schrödinger equation near critical dimension. J. Math. Anal. Appl. **268**(2), 517–549 (2002)
41. Rottschäfer, V., Kaper, T.J.: Geometric theory for multi-bump, self-similar, blowup solutions of the cubic nonlinear Schrödinger equation. Nonlinearity **16**(3), 929–961 (2003)
42. Sulem, C., Sulem, P.-L.: The nonlinear Schrödinger equation: self-focusing and wave collapse. In: Applied Mathematical Sciences, vol. 139. Springer, New York (1999)
43. Tsutsumi, Y.: L^2-solutions for nonlinear Schrödinger equations and nonlinear groups. Funkcial. Ekvac. **30**(1), 115–125 (1987)
44. Weinstein, M.I.: Nonlinear Schrödinger equations and sharp interpolation estimates. Comm. Math. Phys. **87**(4), 567–576 (1982/83)
45. Yang, K., Roudenko, S., Zhao, Y.: Blow-up dynamics and spectral property in the L^2-critical nonlinear Schrödinger equation in high dimensions. Nonlinearity **31**(9), 4354–4392 (2018)
46. Yang, K., Roudenko, S., Zhao, Y.: Blow-up dynamics in the mass super-critical NLS equations. Phys. D **396**, 47–69 (2019)
47. Yang, K., Roudenko, S., Zhao, Y.: Stable blow-up dynamics in the L^2-critical and L^2-supercritical generalized Hartree equations. Stud. Appl. Math. **145**(4), 647–695 (2020)

Terms and Conditions

Springer Nature journal content, brought to you courtesy of Springer Nature Customer Service Center GmbH ("Springer Nature").

Springer Nature supports a reasonable amount of sharing of research papers by authors, subscribers and authorised users ("Users"), for small-scale personal, non-commercial use provided that all copyright, trade and service marks and other proprietary notices are maintained. By accessing, sharing, receiving or otherwise using the Springer Nature journal content you agree to these terms of use ("Terms"). For these purposes, Springer Nature considers academic use (by researchers and students) to be non-commercial.

These Terms are supplementary and will apply in addition to any applicable website terms and conditions, a relevant site licence or a personal subscription. These Terms will prevail over any conflict or ambiguity with regards to the relevant terms, a site licence or a personal subscription (to the extent of the conflict or ambiguity only). For Creative Commons-licensed articles, the terms of the Creative Commons license used will apply.

We collect and use personal data to provide access to the Springer Nature journal content. We may also use these personal data internally within ResearchGate and Springer Nature and as agreed share it, in an anonymised way, for purposes of tracking, analysis and reporting. We will not otherwise disclose your personal data outside the ResearchGate or the Springer Nature group of companies unless we have your permission as detailed in the Privacy Policy.

While Users may use the Springer Nature journal content for small scale, personal non-commercial use, it is important to note that Users may not:

1. use such content for the purpose of providing other users with access on a regular or large scale basis or as a means to circumvent access control;
2. use such content where to do so would be considered a criminal or statutory offence in any jurisdiction, or gives rise to civil liability, or is otherwise unlawful;
3. falsely or misleadingly imply or suggest endorsement, approval , sponsorship, or association unless explicitly agreed to by Springer Nature in writing;
4. use bots or other automated methods to access the content or redirect messages
5. override any security feature or exclusionary protocol; or
6. share the content in order to create substitute for Springer Nature products or services or a systematic database of Springer Nature journal content.

In line with the restriction against commercial use, Springer Nature does not permit the creation of a product or service that creates revenue, royalties, rent or income from our content or its inclusion as part of a paid for service or for other commercial gain. Springer Nature journal content cannot be used for inter-library loans and librarians may not upload Springer Nature journal content on a large scale into their, or any other, institutional repository.

These terms of use are reviewed regularly and may be amended at any time. Springer Nature is not obligated to publish any information or content on this website and may remove it or features or functionality at our sole discretion, at any time with or without notice. Springer Nature may revoke this licence to you at any time and remove access to any copies of the Springer Nature journal content which have been saved.

To the fullest extent permitted by law, Springer Nature makes no warranties, representations or guarantees to Users, either express or implied with respect to the Springer nature journal content and all parties disclaim and waive any implied warranties or warranties imposed by law, including merchantability or fitness for any particular purpose.

Please note that these rights do not automatically extend to content, data or other material published by Springer Nature that may be licensed from third parties.

If you would like to use or distribute our Springer Nature journal content to a wider audience or on a regular basis or in any other manner not expressly permitted by these Terms, please contact Springer Nature at

onlineservice@springernature.com